**USGS AWARD NUMBER: G16AP00138**

**PROJECT DURATION: 12 MONTHS (06/01/2016 THROUGH 05/31/2017)**

**TECHNICAL FINAL REPORT**

# HYBRID EMPIRICAL GROUND-MOTION PREDICTION EQUATIONS FOR THE GULF COAST REGION

S. Pezeshk,[1] A. Zandieh,[2] and A. Haji-Soltani[3]

[1]Department of Civil Engineering
The University of Memphis
Memphis, TN 38152
Phone: (901) 678-4727
Fax: (901) 678-3026
spezeshk@memphis.edu

[2] Lettis Consultants International, Inc.
Boulder, Colorado, 80305
Phone: (901) 692-0431
arash.zandieh@live.com

[3]Mueser Rutledge Consulting Engineers
14 Penn Plaza, 225 West 34th Street
New York, NY 10122
Phone: (646) 581-2232
ahaji-soltani@mcre.com

TABLE OF CONTAENTS

# Hybrid Empirical Ground-Motion Prediction Equations for the Gulf Coast Region

## Introduction

The main purpose of this study is to develop ground motion prediction equations (GMPEs) for the Gulf Coast region of the United States using a hybrid empirical method (HEM). This project contributes toward development of a new set of GMPEs for the Gulf Coast region, which will be consistent with the available recordings. This research supplement recent GMPEs developed by the Pacific Earthquake Engineering Research Center (PEER) Next Generation Attenuation (NGA-East) GMPEs for the Central and Eastern North America (CENA) regions.

For seismic hazard applications, ground-motion amplitudes are often estimated using GMPEs. Prediction of earthquake ground motions for future probable earthquakes is highly demanded for structural design purposes. The GMPEs, also known as attenuation relationships or ground motion models (GMMs), relate ground-motion intensity measures (GMIMs), such as peak ground acceleration (PGA), peak ground velocity (PGV), and 5%-damped pseudo-acceleration linear-elastic response-spectral acceleration (PSA), to seismological parameters in a specified region, such as earthquake magnitude, source-to-site distance, local site conditions, and style-of-faulting. Different approaches have been proposed to develop GMPEs such as empirical methods, stochastic methods, and hybrid empirical method.

GMPEs developed from empirical data are often well constrained, if the database used is comprehensive and complete, and represent the inherent characteristics of ground-motion scaling in the near-source region of large earthquakes. Therefore, empirical methods cannot be used to develop GMPEs that are valid for moderate-to-large magnitudes for regions with limited strong ground-motion data. On the other hand, GMPEs obtained from stochastic point-source models directly may lack realistic near-source characteristics, especially such magnitude-scaling effects as saturation of ground motion with increasing magnitude and decreasing distance, because of the assumption that the total seismic energy is released from a single point within the crust. As a result, in areas with limited ground-motion recordings (e.g., the Gulf Coast region) the hybrid empirical method approach is an appropriate option to develop GMPEs.

The Gulf Coast region is a wide sedimentary area in the central United States. It is centrally located between the eastern Rocky Mountains (western side) and the Appalachian Mountains (eastern side). It also includes the New Madrid seismic zone within the Mississippi embayment (Dreiling *et al*. 2014), which is considered to be an active seismic zone (Nuttli, 1973; Johnston and Schweig, 1996; Tuttle and Schweig, 1999). The Mississippi embayment is made up of overlaid unconsolidated coastal plain sediments that are about 1 km thick at deepest sections (Stearns, 1957; Stearns and Marcher, 1962). The striking characteristics of these sediments with specific seismological properties have been the center of interest in numerous studies in seismology (e.g., Gomberg *et al*., 2003; Cramer, 2006). As is well known, the existence of thick, unconsolidated sediments can amplify seismic waves, which could increases the ground-motion intensity.

The hybrid empirical method (HEM) uses stochastically simulated ground motion intensity measures (GMIMs) in the host and target regions to develop adjustment factors that are applied to empirical GMIM predictions in the host region. In this approach, GMIMs in a target region are predicted from empirical GMPEs in a host region using adjustment factors obtained based on difference between seismological characteristics of the two regions. The adjustment factors are calculated as the ratio of stochastically simulated GMIMs in the two regions. Using appropriate regional seismological parameters in the stochastic simulations, the calculated adjustment factors take into account differences in earthquake source, wave-propagation, and site-response characteristics between the two regions. The empirically derived GMPEs for the host region are mapped to the target region by applying the regional adjustment factors. Hybrid empirical method is widely used to develop GMPEs as an alternative to empirical methods, particularly in the regions where earthquake records of engineering significance are scarce (e.g., Campbell, 2003, 2007, 2008, 2011; Pezeshk *et al*., 2011; Pezeshk *et al*., 2015).

Recently, a number of GMPEs for CENA are developed as part of NGA-East project conducted by the PEER. However, in majority of them, ground motions recorded in the Gulf Coast region were excluded due to considerably different attenuation attributes in this region (EPRI, 1993). As it was discussed earlier, the Gulf Coast region exhibits significantly different ground-motion attenuation because of the thick sediments in the region (Dreiling *et al*. 2014). The purpose of this study is to develop specific GMPEs for use in the Gulf Coast region using the HEM. Because the strong motion data set is sparse in the Gulf Coast region, the hybrid empirical method represent an appropriate and robust approach which has been generally accepted to develop GMPEs.

**Methodology**

In this study, we use the HEM approach to develop new GMPEs for the Gulf Coast region of the United States as the target region. A similar approach used by Pezeshk *et al.* (2015) in developing GMPEs for CENA excluding the Gulf Coast region is employed for this study. The method uses five new empirical GMPEs developed by the PEER center for the NGA-West2 project to estimate GMIMs in the host region. The proposed GMPEs is derived for PGA and 5%-damped PSA at periods ranging from 0.01 to 10 sec, moment magnitudes (**M**) ranging from 3.5 to 8.0, and shortest distances to the fault-rupture surface ($R_{RUP}$) as far as 1000 km from the site, although we caution that the GMPEs are best constrained for $R_{RUP}$ < 300–400 km. The predicted GMIMs are for a reference site defined as the Gulf Coast region hard-rock with $V_{S30}$ = 3,000 m/sec and $\kappa_0$ = 0.006 sec, where $V_{S30}$ is the time-averaged shear-wave velocity in the top 30 m of the site profile and $\kappa_0$ is the total attenuation of the ground motion as it propagates through the site profile Hashash *et al.* (2014a).

The set of seismological parameters used to derive the GMIM stochastic estimates in the Gulf Coast target region are adopted from the most recent research and published information for the region. The seismological parameters for the western North America (WNA) host region are adopted from a point-source inversion of the median GMIM predictions from the NGA-West2 GMPEs for events and sites with 3.5<**M** ≤ 8.0, $R_{RUP}$ ≤ 300 km, NEHRP B/C site conditions with $V_{S30}$ = 760 m/sec, strike-slip style of faulting on a vertical (90°-dipping) fault plane, and earthquake-depth and sediment-depth parameters equal to the default values recommended by the NGA-West2 developers (Zandieh, *et al*., 2017 [hereafter referred to as PZC2017]).

**Stochastic Ground-Motion Simulation**

In the stochastic method, the ground-motion acceleration is modeled as filtered Gaussian white noise modulated by a deterministic envelope function defined by a specified set of seismological parameters (Boore, 2003). The filter parameters are determined by either matching the properties of an empirically defined spectrum of strong ground-motion with theoretical spectral shapes or using reliable physical characteristics of the earthquake source and propagation media (Hanks and McGuire, 1981; Boore, 1983, 2003). A set of computer routines developed by the authors for use in their Pezeshk *et al.* (2015), which is based on the random vibration method of Kottke and Rathje (2008), is used to perform the point-source stochastic simulation of GMIM amplitudes using the WNA and the Gulf Coast region seismological

models. The regional adjustment factors will be the ratio of the simulated spectral values for the Gulf Coast region with respect to those for WNA.

**Spectral Amplitude**

In the point-source model, the total Fourier amplitude spectrum (FAS) of the horizontal vibratory ground displacement, $Y(M_0, R, f)$, due to shear-wave propagation can be modeled by (Boore, 2003):

$$Y(M_0, R, f) = S(M_0, f)P(R, f)G(f)I(f) \quad (1)$$

where $M_0$ is seismic moment (dyne-cm), $R$ is source-to-site distance (km), $f$ is frequency (Hz), $S(M_0,f)$ is the source spectrum, $P(R, f)$ is the path attenuation term, $G(f)$ is the site-response term, and $I(f)$ is a filter representing the type of GMIM.

**Source Term**

We will use the Brune (1970, 1971) $\omega^2$ source spectrum in the stochastic simulations. Brune's model is a single-corner frequency ($f_0$) point-source spectrum in which the stress parameter, $\Delta\sigma$, controls the spectral shape at high frequencies:

$$S(M_0, f) = \frac{R_{\theta\varphi} FV}{4\pi\rho\beta^3} \frac{M_0(2\pi f)^2}{1 + (\frac{f}{f_0})^2} \quad (2)$$

in which $M_0$ is the seismic moment, $R_{\theta\varphi}$ is the radiation pattern, $F$ is the free surface amplitude amplification, $V$ is the coefficient for partitioning into two horizontal components, and $\rho$ is the density. The parameter $f_0$ is the source corner frequency given by:

$$f_0 = 4.906 \times 10^3 \beta (\frac{\Delta\sigma}{M_0})^{1/3} \quad (3)$$

where $\beta$ is the shear-wave velocity at the source and $\Delta\sigma$ is the stress drop.

It is important to note that all seismological parameters (stress parameter, kappa, geometrical spreading, and anelastic attenuation) that are used for this study must be self-consistent and well correlated. Boore *et al.* (2010) showed that estimates of the stress parameter ($\Delta\sigma$) are strongly correlated to the rate of

geometrical spreading in the near-source region. In a related research, ZPC2017 were able to successfully perform an inversion technique to determine WNA seismological parameters using synthetic data from the NGA-West2 GMPEs. The inversion for WNA seismological parameters provide a set of seismological parameters that can be used in the development of a HEM GMPE for this study. Details are provided later in this report.

**Source and Path Duration**

The sum of the source duration and the path duration represents the total duration of ground motion in the stochastic method. The source duration for the Brune single-corner frequency model is typically defined (e.g., Boore, 2003) as the inverse of the source corner frequency, $1/f_0$. We used the path-duration terms proposed by Boore and Thompson (2014, 2015) in this study, which are provided in Table 1 for completeness.

**Path Term**

The path term $P(R, f)$ in Equation (1) is separated into two components, commonly referred to as geometric spreading and anelastic attenuation. Geometric spreading models the amplitude decay due to the expanding surface area of the wave front as it propagates away from the source. Anelastic attenuation, quantified by the quality factor $Q$, models the amplitude decay due to the conversion of elastic wave energy to heat and is usually found to be frequency dependent.

**Path Attenuation for the Gulf Coast region**

For this study, we used the path-attenuation term developed by Chapman *et al.* (2014) for the Gulf Coast region. These authors used broadband recordings from the EarthScope Transportable Array (TA Array) and an iterative inversion process to derive a trilinear geometric attenuation model with $R^{-1.3}$ spreading to 60 km, $R^0$ or no spreading from 60 to 120 km, and $R^{-0.5}$ or $L_g$ spreading beyond 120 km. Chapman *et al.* (2014) found that for the Gulf Coast region the quality factor that is consistent with the above geometric attenuation term is given by the relationship $Q = 365\, f^{0.624}$.

**Path Attenuation for WNA**

We used the path-attenuation terms determined from the inversion of the NGA-West2 GMPEs by ZPC2017.

The geometrical attenuation or spreading term is defined by a piecewise function given by the equation (after Boore, 2003):

$$Z(R) = \begin{cases} R^{b_1} & R \le R_1 \\ Z(R_1)\left(R/R_1\right)^{b_2} & R_1 < R \le R_2 \\ \vdots & \\ Z(R_{n-1})\left(R/R_{n-1}\right)^{b_n} & R > R_n \end{cases} \quad (4)$$

where the values of $b_i$ represent the rates of decay (spreading coefficients) over the specified distance ranges. In this study, we used a trilinear functional forms ($n = 3$) to model $Z(R)$. For the trilinear model, the slope parameters $b_1$ ,$b_2$ and $b_3$ are determined in the inversion and the distance parameters $R_1$ and $R_2$ are set equal to the hinge points in the trilinear WNA path duration model of Boore and Thompson (2014, 2015), resulting in transition distances of $R_1$ = 45 km and $R_2$ = 125 km. The same transition distances are used for the geometric-attenuation and path-duration models because the rate of decay of seismic waves should correlate with the duration of these waves. For the stable continental region (SCR) of CENA, the value of $b_3$ is typically assumed to be associated with the decay of $L_g$ waves at regional distances and usually is set to a fixed value of –0.5. This is not necessarily the case for active crustal regions (ACRs) typically of the WNA. Therefore, ZPC2017 obtained the coefficient $b_3$ by the inversion process consistent with coefficients $b_1$ and $b_2$ to capture the distance decay predicted by NGA-West2 GMPEs. Table 2 summarizes the values of $b_1$ ,$b_2$ and $b_3$ as a function of magnitude and frequency. Figure 1 shows $b_1$ ,$b_2$ and $b_3$ as a function of magnitude and frequency.

The anelastic attenuation parameters, $Q_0$ and $\eta$ , have values that are strongly dependent on the geometric spreading coefficient at large distances, characterized by the parameters $b_2$ and especially $b_3$ in this study. $Q_0$ and $\eta$ parameters used in this study are obtained from ZPC2017 and are listed in Table 2. These parameter values along with the quality factor function $Q(f) = Q_0 f^{\eta}$ are shown in Figure 2. The values of $Q_0$ range from 226 to 276 and those of $\eta$ ranges from 0.55 to 0.63 for different magnitudes.

**Effective Point-Source Distance in the Gulf Region**

In the stochastic point-source model, the earthquake source is assumed to be concentrated at a point within the crust, which is a reasonable assumption for small earthquakes or when the source-to-site distance is considerably larger than the earthquake source dimensions. Otherwise, finite-fault effects in the form of magnitude and distance saturation begin to influence the ground motions. Atkinson and Silva (2000) defined an effective point-source distance metric, $R'_{RUP}$, to be used in point-source stochastic simulations to mimic the ground-motion saturation effects from finite-fault effects. They also defined a magnitude-dependent equivalent point-source depth, $h$, to modify this distance for magnitude-saturation effects. Following these authors, we define an effective point-source distance metric to use with our point-source stochastic simulations with the expression:

$$R'_{RUP} = \sqrt{R_{RUP}^2 + h^2} \tag{5}$$

where the pseudo-depth, *h*, also referred to as the finite-fault factor by Boore and Thompson (2014), is defined by expression:

$$\log h = \begin{cases} \max(-0.05 + 0.15\mathbf{M}, -1.72 + 0.43\mathbf{M}) & \mathbf{M} \le 6.75 \\ -0.405 + 0.235\mathbf{M} & \mathbf{M} > 6.75 \end{cases} \tag{6}$$

**Effective Point-Source Distance in WNA**

We used the effective-depth parameter *h* directly from the inversion obtained by ZCP2017. A summary of *h* values as a function of moment magnitude is tabulated in Table 2 and shown in Figure 3.

**Stress Parameter in the Gulf Coast Region**

Boore and Thompson (2015) found that a stress parameter of 400 bars was needed to approximate the amplitude of the ground motions in CENA. Since we will be using the new path duration model of Boore and Thompson (2015), we used $\Delta\sigma$ = 400 bars for the Gulf Coast region point-source stochastic simulations. This is consistent with the procedure used by Pezeshk *et al.* (2015).

**Stress Parameter in WNA**

We used the stress parameter derived by ZPC2017 from an inversion of the NGA-West2 GMPEs for earthquake scenarios with **M** ≤ 8.0. ZCP2017 obtained average stress drops that increase from 80 bars at **M** 3.5 to about 230 bars at **M** 5.0-5.5 and then decreases to 90 bars at **M** 8.0 for the NGA-West2 GMPEs with an average hypocentral depth of around 9 km (Campbell and Bozorgnia, 2014). Figure 4 shows variation of the stress drop as a function of the magnitude. Table 2 tabulates the stress parameter as a function of magnitude.

**Site Term**

The site-response term $G(f)$ is defined as the product of crustal-amplification and diminution functions (Boore, 2003). Crustal amplification is calculated using the quarter-wavelength (QWL) method, which Boore (2013) now refers to as the square-root-impedance (SRI) method. Boore (2003) proposes the maximum frequency filter, $f_{max}$ (Hanks, 1982), and the kappa filter, $\kappa_0$ (Anderson and Hough, 1984), as alternatives to model the site diminution function. The kappa filter, $\exp(-\pi\kappa_0 f)$, can be considered the path-independent loss of energy in the ground motion as it propagates through the site profile. It is defined by Anderson and Hough (1984) as the high-frequency slope of the FAS on a log-linear plot. We use $\kappa_0$ to define the site attenuation because of its common use in engineering seismology (Campbell, 2009; Ktenidou *et al.*, 2014).

**Reference Rock and Kappa for the Gulf Coast region**

For the Gulf Coast region, we will adopt the reference hard-rock site condition recommended by Hashash *et al.* (2014a) for use in the NGA-East project that corresponds to $V_{S30}$ = 3000 m/sec and $\kappa_0$ = 0.006 sec based on the comprehensive studies of Hashash *et al*. (2014b) and Campbell *et al*. (2014). We used the crustal-amplification factors derived by Boore and Thompson (2015) using the QWL or SRI method, which are based on the velocity profile of Boore and Joyner (1997) modified to have a shear-wave velocity of 3,000 m/sec over the top 300 m of the profile in order to be consistent with the NGA-East reference hard-rock crustal profile of Hashash *et al.* (2014a). These crustal-amplification factors are listed Table 3.

**Reference Rock and Kappa for WNA**

For this study, we used the $\kappa_0$ model that was derived by Zandieh *et al.* (2016) from the high-frequency shape of the NGA-West2 GMPEs. They used the inverse random vibration theory (IRVT) approach described by Al Atik *et al.* (2014) to calculate FAS from predicted values of response-spectral acceleration for all of the NGA-West2 GMPEs. They used these spectra to estimate $\kappa_0$ using the spectral-decay method of Anderson and Hough (1984). NGA-West2 GMPEs were evaluated for a NEHRP B/C site condition and for default estimates of depth to the top of rupture, hypocentral depth, and sediment (basin) depth, consistent with this study. They derived estimates of $\kappa_0$ for magnitudes ranging from 3.5 to 8.0 and distances ranging from 5 to 20 km and used a mixed-effects model to derive equations for $\kappa_0$ as a function of magnitude. One of the main goals of Zandieh *et al.* (2016) study was to develop a $\kappa_0$ model that could be used in inversions to develop stochastic models that are intended to mimic the predictions from the NGA-West2 GMPEs. For this study, the $\kappa_0$ from Model 2 in Zandieh *et al.* (2016) is adopted. Model 2 of Zandieh *et al.* (2016) is the most representative of the average trend in the values of $\kappa_0$ with magnitude if the weighted geometric mean of all five of the NGA-West2 GMPEs and is used to define the GMIMs, with weights that are the same as used by Petersen *et al*. (2014). The $\kappa_0$ Model 2 in Zandieh *et al*. (2016) is given by the equation:

$$\kappa_0 = \begin{cases} 0.03367; & \mathbf{M} \le 4.4377 \\ 0.03367 + 0.00773(\mathbf{M} - 4.4377); & 4.4377 < \mathbf{M} < 5.8794 \\ 0.04481; & \mathbf{M} \ge 5.8794 \end{cases} \quad (7)$$

**Empirical GMPEs for WNA**

We used the five GMPEs developed as part of the PEER NGA-West2 project (Bozorgnia *et al.*, 2014) to derive the empirical GMIM estimates in the WNA host region. These GMPEs are referred to as ASK14 (Abrahamson *et al.*, 2014), BSSA14 (Boore *et al.*, 2014), CB14 (Campbell and Bozorgnia, 2014), CY14 (Chiou and Youngs, 2014), and I14 (Idriss, 2014) in the remainder of this report. We used the weighted average (in logarithmic space) of horizontal spectral accelerations from the five GMPEs in order to derive empirical estimates for WNA. The spectral accelerations from NGA-West2 GMPEs are expressed as RotD50 Boore (2010). These accelerations are consistent with the inversions performed by ZPC2017.

The same weights were assigned that were used to evaluate the NGA-West2 GMPEs for the 2014 update of the U.S. national seismic hazard model (Petersen *et al*., 2014).

## Ground Motion Prediction Equations for the Gulf Coast region

Median estimates of the desired GMIMs in the Gulf Coast region will be obtained by scaling the NGA-West2 empirical estimates of PGA and PSA with the stochastically derived adjustment factors derived using stochastic simulations with the sets of seismological parameters appropriate for both the target and the host regions as discussed earlier. The GMIMs will be evaluated for 9 values of magnitude ranging from **M** = 3.5–8.0 in 0.5 magnitude increments and for 25 values of distance given by the array $R_{RUP}$ = 1, 2, 5, 10, 15, 20, 30, 40, 50, 60, 70, 80, 100, 120, 140, 180, 200, 250, 300, 400, 500, 600, 700, 800, and 1000 km. Since the GMPEs will be developed for a reference hard-rock site with $V_{S30}$ = 3000 m/sec and $\kappa_0$ = 0.006 sec (Hashash *et al.*, 2014a), the GMIM predictions must be modified for other site conditions using an appropriate site-response method.

The HEM-simulated GMIMs will be used together with nonlinear least-squares regression to derive the model coefficients in a GMPE defined with a specified functional form. GMPEs will be developed for PGA and for 5%-damped PSA for **M** ≤ 8, $R_{RUP}$ ≤ 1,000 km, and 21 spectral periods ranging from $T$ = 0.01–10 sec, consistent with the set of periods used in the NGA-West2 models. The following GMPE functional form expression used for this study:

$$\begin{aligned}\log(\overline{Y}) = {} & c_1 + c_2\mathbf{M} + c_3\mathbf{M}^2 + \left(c_4 + c_5\mathbf{M}\right)\times \min\left[\log(R),\log(60)\right] \\ & + \left(c_6 + c_7\mathbf{M}\right)\times \max\left[\min\left\{l\,\mathrm{og}(R/60),\log(120/60)\right\},0\right] \\ & + \left(c_8 + c_9\mathbf{M}\right)\times \max\left[\log(R/120),0\right] + c_{10}R\end{aligned} \tag{8}$$

where

$$R = \sqrt{R_{RUP}^2 + C_{11}^2} \tag{9}$$

In these equations, $\overline{Y}$ is the median value of PGA or PSA ($g$), **M** is the moment magnitude, and $R_{RUP}$ is the closest distance to the fault-rupture surface (km). Coefficients $C_1$ through $C_{11}$ are tabulated in Table 4.

**Aleatory and Epistemic Uncertainty Considerations**

The aleatory variability characterizes the inherent randomness in the predicted GMIMs that results from any unmodeled characteristics of the ground motion (Campbell, 2007). In this study, we constructed the mean aleatory variability model from the weighted average of the standard deviations of the five NGA-West2 GMPEs, similar to the approach of Campbell (2003, 2007), Tavakoli and Pezeshk (2005), Pezeshk *et al*., (2011), and Pezeshk *et al.*, (2015). Except for I14, the other four NGA-West2 GMPEs partition the total standard deviation, $\sigma$, into components that represent between-event variability ($\tau$) and within-event variability ($\phi$). We used the weighted average of the between-event and within-event standard deviations from these four NGA-West2 models to derive the aleatory variability model proposed in this study. All of the NGA-West2 GMPEs have standard deviations that vary with magnitude and some that vary with distance and site conditions. Since the GMPEs were evaluated for firm-rock site conditions, the dependence on site conditions could be neglected. Also, because of the relatively weak distance-dependence of the average standard deviations, we chose to simplify the model by excluding distance as a parameter and instead averaged the standard deviations over the 25 distance values used to evaluate the NGA-West2 GMPEs for each magnitude. The resulting natural log standard deviations are given by the expressions:

$$\tau = \begin{cases} c_{12} & \mathbf{M} \le 4.5 \\ c_{13} + c_{14}\mathbf{M} & 4.5 < \mathbf{M} \le 5.0 \\ c_{15} + c_{16}\mathbf{M} & 5.0 < \mathbf{M} \le 6.5 \\ c_{17} + c_{18}\mathbf{M} & \mathbf{M} > 6.5 \end{cases} \tag{10}$$

and

$$\phi = \begin{cases} c_{19} + c_{20}\mathbf{M} & \mathbf{M} \le 4.5 \\ c_{21} + c_{22}\mathbf{M} & 4.5 < \mathbf{M} \le 5.0 \\ c_{23} + c_{24}\mathbf{M} & 5.0 < \mathbf{M} \le 6.5 \\ c_{25} & \mathbf{M} > 6.5 \end{cases} \tag{11}$$

$C_{13}$ through $C_{18}$ are tabulated in Table 5. $C_{19}$ through $C_{25}$ are tabulated in Table 6 . The total aleatory standard deviation, excluding the variability of the regression, is calculated from the between-event and within-event standard deviations by the equation:

$$\sigma = \sqrt{\tau^2 + \phi^2} \tag{12}$$

The total aleatory standard deviation that includes the variability of the regression is given by the equation:

$$\sigma_T = \sqrt{\sigma^2_{\log \bar{Y}} + \sigma^2_{\mathrm{Reg}}} \tag{13}$$

Standard deviation of the regression, $\sigma_{\mathrm{Reg}}$, is provided in Table 4. The model misfit is much smaller than the other aleatory variability components and can be neglected for many seismic-hazard applications (e.g., Pezeshk *et al*., 2011). Based on the mathematical framework given in Campbell (2003), the major sources of epistemic uncertainty in the HEM approach are due to: (1) uncertainty in the seismological parameters used in the stochastic simulations, and (2) uncertainty in the empirical GMPEs. Epistemic uncertainty is not included in this study. This type of uncertainty is typically evaluated by using alternative GMPEs and the within-model uncertainty associated with an individual GMPE, such as that proposed by Al Atik and Youngs (2014). The epistemic uncertainty is not usually included in HEM approach (e.g., Campbell, 2007, 2014; Pezeshk *et al*., 2011; Pezeshk *et al.,* 2015).

## Comparison with Observations

The GMIM predictions from the GMPEs developed in this study are compared to the PGA and PSA values from the NGA-East database (Goulet *et al.*, 2014) for available recordings with **M** ≥ 3.0 and $R_{RUP}$ < 1000 km. Figure 6 displays the magnitude-distance distribution of the selected recordings.

Figure 6 shows the boundary of the Gulf Coast region as defined by the NGA-East researchers (Dreiling *et al.,* 2014). Figure 6 also displays a map of the recording stations with different colors representing their NEHRP site class and also displays a map of the associated earthquakes. NEHRP site class E (soft-soil) sites are excluded from consideration because of their complex site-response characteristics and their potential for significant nonlinear site effects. As seen in Figure 6, the selected recordings could be obtained on a variety of site conditions. All the earthquakes located within the Gulf Coast boundary and some that are close to the Gulf Coast region are considered.

To perform a consistent comparison between the GMIM predictions from the GMPE developed in this study and the observations, the observed GMIMs will be adjusted to the CENA hard-rock reference site condition used to develop the GMPE based on the same approach used in the NGA-East project by Pezeshk *et al.* (2015). A summary of the method that we used to adjust the observations to the CENA reference hard-rock site condition can be described as follows:

1. Compile generic $V_S$ and density profiles corresponding to $V_{S30}$ = 760 m/sec (Atkinson and Boore, 2006), $V_{S30}$ = 2000 m/sec (Atkinson and Boore, 2006), and $V_{S30}$ = 3000 m/sec (Boore and Thompson, 2015);
2. For each recording of given **M**, $R_{RUP}$, and $V_{S30}$ < 1500 m/sec, correct the record to the $V_{S30}$ = 760 m/sec site condition using the empirical site term in Boore *et al.* (2014) and the value of rock *PGA* from the CENA stochastic simulations. For the few sites with 1500 < $V_{S30}$ < 2000 m/sec, it is assumed that the records are consistent to the site condition represented by the $V_{S30}$ = 2000 m/sec site profile (no adjustment is performed).
3. Find the ratio of stochastically derived PGA and PSA values for the $V_{S30}$ = 760 and $V_{S30}$ = 3000 m/sec site profiles or between the $V_{S30}$ = 2000 and $V_{S30}$ = 3000 m/sec site profiles and use these as adjustment factors to correct the recorded GMIM values obtained in step 2 to the reference hard-rock site conditions.

Figure 7 compares the site factors that were used to adjust the observed PSA values from the reference NEHRP B/C site condition, or alternatively from the Atkinson and Boore (2006) hard-rock site condition, to the CENA reference hard-rock site condition, which includes the effects of both crustal amplification and site attenuation. The plots show the spectral ratio of PSA between the $V_{S30}$ = 760 and $V_{S30}$ = 3000 m/sec site profiles (top plot) and between the $V_{S30}$ = 2000 and $V_{S30}$ = 3000 m/sec site profiles (bottom plot). Ratios are given for **M** = 3.5, 4.5, 5.5, and 6.5 and $R_{RUP}$ = 10 and 100 km. The magnitude range was selected in order to show the adjustment factors that are most relevant to the magnitudes of the observed earthquakes. The two distances are provided to demonstrate how the adjustment factors vary with distance. These plots show that the adjustments can be relatively large for the NEHRP B/C site profile and almost negligible for the $V_{S30}$ = 2000 m/sec site profile.

Figure 8 compares the median predicted values of PSA from the GMPE based on stochastic scaling at large magnitudes versus the site-adjusted observed PSA at $T$ = 0.2, 1.0, and 2.0 sec for three one-unit magnitude bins centered at **M** = 3.5, 4.0, and 4.5. These comparisons include the common log empirical calibration constants to adjust the GMIM predictions from the GMPE for the average misfit between the predictions and the observations over all magnitudes, distances, and spectral periods. In general, there is

relatively good agreement between the PSA predictions and the observations, although there are some magnitudes and distances where the comparison is better than others. We note that there is a great deal of uncertainty associated with adjusting the observed GMIMs to the reference hard-rock site conditions in the Gulf Coast region that precludes making definitive conclusions regarding their comparison with the predicted values.

Figure 9 shows the total residuals from the GMIM predictions that are based on stochastic scaling at large magnitudes as a function of distance for $T$ = 0.2, 1.0, and 2.0 sec. In this figure, the size of each circle and its color represents the magnitude of the earthquake. In general, there is no substantial trend in the total residuals with distance.

A variance-component technique proposed by Chen and Tsai (2002) was used to decompose the prediction error of the GMIMs into three components, which using the terminology of Al Atik *et al.* (2010) are: (1) the between-event standard deviation $\tau$, (2) the site-to-site standard deviation $\phi_{S2S}$, and (3) the within-event single-site standard deviation $\phi_{SS}$. Figure 10 displays these residuals for $T$ = 1.0 sec as a function of magnitude and distance. As can be seen in Figure 10, the total residual errors are significantly reduced once they are corrected for the between-event and the site-to-site components of variability.

## Comparison with Existing Models

Figure 11 shows a comparison of the distance-scaling (attenuation) characteristics of the GMPEs developed in this study (hereafter referred to as Gulf) with those of Pezeshk *et al.* (2015) (hereafter referred to as PZCT15-Stochastic and PZCT15-Empirical). Plots are shown for PGA and PSA at $T$ = 0.1, 0.2, 0.5, 1.0, and 4.0 sec, **M** = 4.5 and 7.0, and $R_{RUP}$ = 1–1000 km.

Figure 11 displays the magnitude-scaling characteristics of the PSA predicted by this study (Gulf) for $R_{RUP}$ = 5, 10, 30, and 70 km and compared with the PZCT2015 stochastic-scaling approach. This figure shows that the Gulf model show a bump characteristics in low period range of less than 0.1 sec which is not present for PZCT2015 model for distances up to 70 km.

## Summary

The hybrid empirical method of Campbell (2003) was used to develop a new set of GMPEs for the Gulf Coast of the United States. The new GMPEs are valid for prediction PGA and 5%-damped PSA for $T$ = 0.01–10 sec, **M** = 3.5–8.0, and nominally for $R_{RUP}$ < 1000 km. The GMIM predictions represent the reference hard-rock site condition recommended by Hashash *et al.* (2014a), which corresponds to a site with $V_{S30}$ = 3000 m/sec and $\kappa_0$ = 0.006 sec. The prediction of GMIMs for other site conditions requires using appropriate site-amplification factors, such as those used to adjust the Gulf Coast region recordings to the reference hard-rock site condition in this study. We consider our new GMPE to be a viable alternative to both the existing set of Gulf GMPEs in the development of the national seismic hazard model, and to other GMPEs that are being developed as part of the NGA-East project. This study developed using the HEM approach will be an important contribution to the distribution of epistemic uncertainty of GMIM predictions in the Gulf Coast region.

The application of the HEM approach in this study used WNA empirical GMPEs developed as part of the NGA-West2 project (Bozorgnia *et al.*, 2014) to estimate GMIMs in the host region. These GMPEs were evaluated for a reference firm-rock site condition corresponding to $V_{S30}$ = 760 m/sec and the default earthquake depths and basin effects recommended by the GMPE developers. For the WNA stochastic simulations, we used a consistent set of seismological parameters that were derived from the NGA-West2 GMPEs (Zandieh *et al*., 2017). For the CENA stochastic simulations, we used an updated set of internally consistent seismological parameters. The major assumption in the HEM approach is that the near-source scaling and saturation effects observed in active tectonic regions, such as WNA, is a general behavior that can be extended to other tectonic regions, such as the Gulf Coast region. The empirical GMIM predictions from the host region were adjusted by stochastically simulated GMIM ratios that account for the differences in the source, path, and site response between the target (Gulf) and the host (WNA) regions. These adjustment factors were evaluated using a point-source stochastic model with an effective point-source distance metric that mimics the distance from a finite-fault rupture plane, such as that used in the NGA-West2 GMPEs.

The GMIM predictions from the GMPEs developed in this study were compared with the observed GMIM values from the NGA-East database (Goulet *et al*., 2014; see Data and Resources Section) by evaluating the residuals between the predictions and the observations, after adjusting the latter to the reference hard-rock site condition (Hashash *et al.*, 2014a). In general, there is relatively good agreement between the GMPEs and the Gulf Coast region observations. We consider any disagreement between the predictions and site-adjusted observations to be acceptable, considering the relatively large

adjustments and associated uncertainty that was necessary to adjust the observations to the reference hard-rock site condition.

Finally, the developed GMPEs can be used in the upcoming USGS hazard map updates, and also could be used in PSHA projects performed in the Gulf Coast region (e.g., Haji-Soltani, 2017, Haji-Soltani and Pezeshk, 2017a, b). For the vertical response spectra, the developed GMPEs could be used along with the Haji-Soltani *et al.* (2017) V/H ratios for the sites located within the Gulf Coast region, which include the Mississippi embayment.

## References


Abrahamson, N. A., W. J. Silva, and R. Kamai (2014). Summary of the ASK14 ground motion relation for active crustal regions, *Earthq. Spectra* **30**, 1025–1055.

Anderson, J. G., and S. E. Hough (1984). A model for the shape of the Fourier amplitude spectrum of acceleration at high frequencies, *Bull. Seism. Soc. Am*. **74**, 1969–1993.

Al Atik, L., and R. R. Youngs (2014). Epistemic uncertainty for NGA-West2 models, *Earthq. Spectra* **30**, 1301–1318.

Al Atik, L., A. Kottke, N. A. Abrahamson, and J. Hollenback (2014). Kappa ($\kappa$) scaling of ground-motion prediction equations using an inverse random vibration theory approach, *Bull. Seismol. Soc. Am*. **104**, 336–346.

Al Atik, L., N. Abrahamson, J.J. Bommer, F. Scherbaum, F. Cotton, and N. Kuehn (2010). The variability of ground-motion prediction models and its components, *Seismol. Res. Lett*. **81**, 794–801.

Atkinson, G. M. (2004). Empirical attenuation of ground motion spectral amplitudes in southeastern Canada and the northeastern United States, *Bull. Seismol. Soc. Am*. **94**, 1079–1095.

Atkinson, G. M., and K. Assatourians (2010). Attenuation and source characteristics of the 23 June 2010 **M** 5.0 Val-des-Bois, Quebec, earthquake, *Seismol. Res. Lett.* **81**, 849–860.

Atkinson, G. M., and D. M. Boore (1995). New ground motion relations for eastern North America, *Bull. Seismol. Soc. Am.* **85**, 17–30.

Atkinson, G. M., and D. M. Boore (1998). Evaluation of models for earthquake source spectra in eastern North America, *Bull. Seismol. Soc. Am*. **88**, 917–934.

Atkinson, G. M., and D. M. Boore (2006). Ground motion prediction equations for earthquakes in eastern North America, *Bull. Seismol. Soc. Am*. **96**, 2181–2205.

Atkinson, G. M., and D. M. Boore (2011). Modifications to existing ground-motion prediction equations in light of new data, *Bull. Seismol. Soc. Am*. **101**, 1121–1135.

Atkinson, G. M., and W. Silva (1997). An empirical study of earthquake source spectra for California earthquakes, *Bull. Seismol. Soc. Am*. **87**, 97–113.

Atkinson, G. M., and W. Silva (2000). Stochastic modeling of California ground motions, *Bull. Seismol. Soc. Am*. **90**, 255–274.

Atkinson, G. M., and D. J. Wald (2007). Did you feel it? Intensity data: A surprisingly good measure of earthquake ground motion, *Bull. Seismol. Soc. Am*. **78**, 362–368.

Atkinson, G. M., D. M. Boore, K. Assatourians, K. Campbell, and D. Motazedian (2009). A guide to differences between stochastic point-source and stochastic finite-fault simulations, *Bull. Seismol. Soc. Am*. **99**, 3192–3201.

Boore, D. M. (1983). Stochastic simulation of high-frequency ground motion based on seismological models of the radiated spectra, *Bull. Seismol. Soc. Am.* **73**, 1865–1893.

Boore, D. M. (2003). Prediction of ground motion using the stochastic method, *Pure Appl. Geophys.* **160**, 635–676.

Boore, D. M. (2005). SMSIM—Fortran Programs for Simulating Ground Motions from Earthquakes: Version 2.3–A Revision of OFR 96-80-A, *U.S. Geol. Surv. Open-File Rept. 00–509, Revised 15 August 2005*, 55 pp.

Boore, D. M. (2009). Comparing stochastic point-source and finite-source ground-motion simulations: SMSIM and EXSIM, *Bull. Seismol. Soc. Am.* **99**, 3202–3216.

Boore, D. M. (2010). Orientation-independent, nongeometric-mean measures of seismic intensity from two horizontal components of motion, *Bull. Seismol. Soc. Am*. **100**, 1830–1835.

Boore, D. M. (2013). The uses and limitations of the square-root-impedance method for computing site amplification, *Bull. Seismol. Soc. Am.* **103**, 2356–2368.

Boore, D. M., and W. B. Joyner (1997). Site amplification for generic rock sites, *Bull. Seismol. Soc. Am*. **87**, 327–341.

Boore, D. M., and E. M. Thompson (2014). Path duration for use in the stochastic-method simulation of ground motions, *Bull. Seismol. Soc. Am.* **104**, 2541–2552.

Boore, D. M., and E. M. Thompson (2015). Revisions to some parameters used in stochastic method simulations of ground motion, *Bull. Seismol. Soc. Am.* **105**, submitted.

Boore, D. M., K. W. Campbell, and G. M. Atkinson (2010). Determination of stress parameters for eight well-recorded earthquakes in eastern North America, *Bull. Seismol. Soc. Am.* **100**, 1632–1645.

Boore, D. M., J. P. Stewart, E. Seyhan, and G. M. Atkinson (2014). NGA-West2 equations for predicting PGA, PGV, and 5% damped PSA for shallow crustal earthquakes, *Earthq. Spectra* **30**, 1057–1085.

Bozorgnia, Y., and 30 other authors (2014). NGA-West2 research project, *Earthq. Spectra* **30**, 973–987.

Brune, J. (1970). Tectonic stress and the spectra of seismic shear waves, *J. Geophys. Res*. **75**, 4997–5009.

Brune, J. (1971). *Correction*: Tectonic stress and the spectra of seismic shear waves, *J. Geophys. Res.* **76**, 5002.

Campbell, K. W. (2003). Prediction of strong ground motion using the hybrid empirical method and its use in the development of ground–motion (attenuation) relations in eastern North America, *Bull. Seismol. Soc. Am.* **93**, 1012–1033.

Campbell, K. W. (2007). *Validation and Update of Hybrid Empirical Ground Motion (Attenuation) Relations for the CEUS*, final report to U.S. Geological Survey, National Earthquake Hazards Reduction External Research Program, Award No. 05HQGR0032.

Campbell, K. W. (2008). Hybrid empirical ground motion model for PGA and 5% damped linear elastic response spectra from shallow crustal earthquakes in stable continental regions: Example for eastern North America. *Proc. 14th World Conference on Earthquake Engineering*, Oct. 12–17, Beijing, China, Paper No. S03-001.

Campbell, K. W. (2009). Estimates of shear-wave $Q$ and $\kappa_0$ for unconsolidated and semiconsolidated sediments in eastern North America, *Bull. Seismol. Soc. Am*. **99**, 2365–2392.

Campbell, K. W. (2011). Ground motion simulation using the hybrid empirical method: Issues and insights, in *Earthquake Data in Engineering Seismology: Predictive Models, Data Management and Networks*, S. Akkar, P. Gulkan, and T. van Eck (eds.), Geotechnical, Geological and Earthquake Engineering Series, Vol. 14, Springer, London, pp. 81–95.

Campbell, K. W. (2014). An evaluation of eastern North America ground-motion models developed using the hybrid empirical method, *Bull. Seismol. Soc. Am.* **104**, 347–359.

Campbell, K. W., and Y. Bozorgnia (2014). NGA-West2 ground motion model for the average horizontal components of PGA, PGV, and 5% damped linear acceleration response spectra, *Earthq. Spectra* **30**, 1087–1115.

Campbell, K. W., Y. M. A. Hashash, B. Kim, A. R. Kottke, E. M. Rathje, W. J. Silva, and J. P. Stewart (2014). *Reference Rock Site Conditions for Central and Eastern North America: Part II – Attenuation (Kappa) Definition*, PEER Report No. 2014/12, Pacific Earthquake Engineering Research Center, University of California, Berkeley, CA, 54 pp.

Chapman, M., S. Pezeshk, M. Hosseini, and A. Conn (2014). Regional study of Fourier amplitude drop of *Lg*-wave acceleration in central United States, *Seismol. Res. Lett*. **85**, 513.

Chen, Y. H., and C.-C. P. Tsai (2002). A new method of estimation of the attenuation relationship with variance components, *Bull. Seismol. Soc. Am.* **92**, 1984–1991.

Chiou, B. S.-J., and R. R. Youngs (2014). Update of the Chiou and Youngs NGA model for the average horizontal component of peak ground motion and response spectra, *Earthq. Spectra* **30**, 1117–1153.

Dreiling J., M. P. Isken, W. D. Mooney, M. C. Chapman, and R. W. Godbee (2014). *NGA-East Regionalization Report: Comparison of Four Crustal Regions within Central and Eastern North America Using Waveform Modeling and 5%-Damped Pseudo-Spectral Acceleration Response*, PEER Report No. 2014/15, Pacific Earthquake Engineering Research Center, University of California, Berkeley, CA.

Electric Power Research Institute (EPRI) (1993). Guidelines for Determining Design Basis Ground Motions. Palo Alto, CA., *Electric Power Research Institute*, 1–5 EPRI TR-102293.

Gomberg, J., P. Bodin, and P. A. Reasenberg (2003). Observing earthquakes triggered in the near field by dynamic deformations, *Bull. Seismol. Soc. Am*. **93**, 118–138.

Goulet, C. A., T. Kishida, T. D. Ancheta, C. H. Cramer, R. B. Darragh, W. J. Silva, Y. M. A. Hashash, J. Harmon, J. P. Stewart, K. E. Wooddell, and R. R. Youngs (2014). *PEER NGA-East Database*, PEER Report No. 2014/17*,* Pacific Earthquake Engineering Research Center, University of California, Berkeley, CA.

Cramer, C. H. (2006). An assessment of the impact of the 2003 EPRI ground-motion prediction models on the USGS national seismichazard maps, *Bull. Seismol. Soc. Am*. **96**, 1159–1169.

Haji-Soltani, A. (2017). A comprehensive site-specific probabilistic seismic hazard analysis for a liquid natural gas tank located in the Gulf Coast region, *Ph.D. Dissertation*, The University of Memphis, Memphis, Tennessee.

Haji-Soltani, A., and S. Pezeshk (2017a). Comparison of different approaches to incorporate site effects and associated uncertainties in probabilistic seismic hazard analysis: application for a liquid natural gas tank, *Annual Meeting of the Seismological Society of America, Denver*, Colorado, 18–20 April.

Haji-Soltani, A., and S. Pezeshk (2017b). A Comparison of Different Approaches to Incorporate Site Effects into PSHA: A Case Study for a Liquefied Natural Gas Tank, Bull. *Seismol. Soc. Am.* (Under review).

Haji-Soltani, A., S. Pezeshk, M. Malekmohammadi, and A. Zandieh (2017). A Study of Vertical to Horizontal Ratio of Earthquake Components in the Gulf Coast Region, *Bull. Seismol. Soc. Am*. (in press).

Hanks, T. C. (1982). $f_{max}$, *Bull. Seismol. Soc. Am*. **72**, 1867–1879.

Hanks, T. C., and R. K. McGuire (1981). The character of high–frequency strong ground motion, *Bull. Seismol. Soc. Am*. **71**, 2071–2095.

Hashash, Y. M. A., A. R. Kottke, J. P. Stewart, K. W. Campbell, B. Kim, C. Moss, S. Nikolaou, E. M. Rathje, and W. J. Silva (2014a). Reference rock site condition for central and eastern North America, *Bull. Seismol. Soc. Am*. **104**, 684–701.

Hashash, Y. M. A., A. R. Kottke, J. P. Stewart, K. W. Campbell, B. Kim, E. M. Rathje, and W. J. Silva, S. Nikolaou, and C. Moss (2014b). *Reference-Rock Site Conditions for Central and Eastern North America: Part I – Velocity Definition*, PEER Report No. 2014/11, Pacific Earthquake Engineering Research Center, University of California, Berkeley, CA, 154 pp.

Johnston, A. C., and E. S. Schweig (1996). The enigma of the New Madrid earthquakes of 1811-1812, *Annu. Rew. Earth. Planet. Sci*. **24**, 339–384.

Kottke, A. R., and E. M. Rathje (2008). *Technical Manual for Strata*, PEER Report No. 2008/10, Pacific Earthquake Engineering Research Center, University of California, Berkeley, CA.

Ktenidou, O. J., F. Cotton, N. A. Abrahamson, and J. G. Anderson (2014). Taxonomy of $\kappa$: A review of definitions and estimation approaches targeted to applications, *Seismol. Res. Lett*. **85**, 135–146.

Idriss, I. M. (2014). An NGA-West2 empirical model for estimating the horizontal spectral values generated by shallow crustal earthquakes, *Bull. Seismol. Soc. Am*. **30**, 1155–1177.

McGuire, R. K., and T. C. Hanks (1980). RMS accelerations and spectral amplitudes of strong ground motion during the San Fernando, California, earthquake, *Bull. Seismol. Soc. Am*. **70**, 1907–1919.

Nuttli, O. W. (1973). The Mississippi Valley earthquakes of 1811 and 1812: intensities, ground motions, and magnitudes, *Bull. Seismol. Soc. Am*. **63**, 227–448.

Petersen, M. D., M. P. Moschetti, P. M. Powers, C. S. Mueller, K. M. Haller, A. D. Frankel, Y. Zeng, , S. Rezaeian, S. C. Harmsen, O. S. Boyd, N. Field, R. Chen, K. S, Rukstales, N. Luco, R. L. Wheeler, R. A. Williams, and A. H. Olsen (2014). Documentation for the 2014 update of the United States national seismic hazard maps: *U.S. Geol. Surv. Open-File Rept. 2014-1091*, 243 pp.

Pezeshk, S., A. Zandieh, and B. Tavakoli (2011). Hybrid empirical ground-motion prediction equations for eastern North America using NGA models and updated seismological parameters, *Bull. Seismol. Soc. Am*. **101**, 1859–1870.

Pezeshk, S., A. Zandieh, K. Campbell, and B. Tavakoli (2015). Ground-motion prediction equations for CENA using the Hybrid Empirical Method in Conjunction with NGA-West2 Empirical Ground-Motion Models, Chapter 5, PEER Report No. 2015/04.

Tavakoli, B., and S. Pezeshk (2005). Empirical-stochastic ground-motion prediction for eastern North America, *Bull. Seismol. Soc. Am*. **95**, 2283–2296.

Tuttle, M. P., and E. S. Schweig (1999). Towards a paleoearthquake chronology for the New Madrid seismic zone, *U.S. Geol. Surv. NEHRP Ann. Rept*., 17 pp.

Yenier, E., and G. M. Atkinson (2014). Equivalent point-source modeling of moderate to large magnitude earthquakes and associated ground-motion saturation effects, Bull. Seismol. Soc. Am. 104, 1458–1478.

Yenier, E., and G. M. Atkinson (2015a). Regionally-adjustable generic ground-motion prediction equation based on equivalent point-source simulations: Application to central and eastern North America, Bull. Seismol. Soc. Am., submitted.

Zandieh, A., Pezeshk, and K. Campbell (2017). The estimation of seismological parameters for use in a stochastic point source model for western United States using an inversion technique to match the median NGA-West2 GMPEs, Bull. Seismol. Soc. Am., under review.

Zandieh, A. K. W. Campbell, and S. Pezeshk. (2016). Estimation of κ0 Implied by the High-Frequency Shape of the NGA-West2 Ground-Motion Prediction Equations, Bulletin of the Seismological Society of America, June, 106:1342-1356; published ahead of print May 24, 2016, doi:10.1785/0120150356.

Table 1. Path-duration models (Boore and Thompson, 2015)

| CENA (used for Gulf coast region in this study) Table 2 of Thompson and Boore (2015) | | WNA Table 1 of Thompson and Boore (2015) | |
|---|---|---|---|
| $R_{RUP}$ (km)* | $T_P$ (sec) | $R_{RUP}$(km) | $T_P$(sec) |
| 0 | 0.0 | 0.0 | 0.0 |
| 15 | 2.6 | 7.0 | 2.4 |
| 35 | 17.5 | 45.0 | 8.4 |
| 50 | 25.1 | 125.0 | 10.9 |
| 125 | 25.1 | 175.0 | 17.4 |
| 200 | 28.5 | 270.0 | 34.2 |
| 392 | 46.0 | | |
| 600 | 69.1 | | |
| Slope of last segment | 0.111 | Slope of last segment | 0.156 |

*Rupture distance must be converted to the effective point-source distance using the pseudo-depth appropriate for each magnitude.

*Table 2. seismological parameter for WNA obtained in ZPC2017 (Source: Zandieh et al. (2017)).*

| **M** | $b_2$ | $b_3$ | $\Delta\sigma$ (bars) | $Q_0$ | $\eta$ | $h$ (km) | $b_1$ | | | | | | | | |
|---|---|---|---|---|---|---|---|---|---|---|---|---|---|---|---|
| | | | | | | | 0.100 Hz | 0.133 Hz | 0.178 Hz | 0.237 Hz | 0.316 Hz | 0.422 Hz | 0.562 Hz | 0.750 Hz | 1.000 Hz |
| 3.5 | -1.171 | -0.679 | 80.895 | 275.531 | 0.559 | 4.244 | -0.873 | -0.876 | -0.828 | -0.823 | -0.851 | -0.868 | -0.902 | -0.920 | -0.969 |
| 4 | -1.034 | -0.655 | 107.559 | 242.216 | 0.571 | 4.674 | -0.897 | -0.900 | -0.881 | -0.878 | -0.912 | -0.924 | -0.961 | -0.978 | -1.018 |
| 4.5 | -0.972 | -0.598 | 150.259 | 226.391 | 0.591 | 5.612 | -0.912 | -0.938 | -0.921 | -0.941 | -0.953 | -0.972 | -1.013 | -1.041 | -1.090 |
| 5 | -0.956 | -0.706 | 233.499 | 244.929 | 0.579 | 6.586 | -0.932 | -0.974 | -0.960 | -0.978 | -1.009 | -1.035 | -1.073 | -1.112 | -1.161 |
| 5.5 | -0.824 | -0.678 | 234.901 | 248.318 | 0.570 | 7.269 | -0.958 | -1.008 | -1.019 | -1.060 | -1.104 | -1.143 | -1.178 | -1.205 | -1.229 |
| 6 | -0.730 | -0.622 | 205.414 | 239.606 | 0.602 | 8.471 | -0.993 | -1.060 | -1.091 | -1.150 | -1.202 | -1.226 | -1.255 | -1.252 | -1.244 |
| 6.5 | -0.652 | -0.554 | 183.268 | 232.763 | 0.626 | 10.084 | -1.033 | -1.132 | -1.183 | -1.232 | -1.275 | -1.280 | -1.281 | -1.264 | -1.248 |
| 7 | -0.579 | -0.516 | 145.210 | 239.410 | 0.592 | 11.871 | -1.142 | -1.248 | -1.275 | -1.294 | -1.304 | -1.303 | -1.294 | -1.269 | -1.245 |
| 7.5 | -0.514 | -0.467 | 122.026 | 240.315 | 0.587 | 13.850 | -1.215 | -1.308 | -1.308 | -1.311 | -1.314 | -1.304 | -1.298 | -1.265 | -1.249 |
| 8 | -0.403 | -0.560 | 93.484 | 270.323 | 0.546 | 15.145 | -1.226 | -1.289 | -1.288 | -1.289 | -1.292 | -1.292 | -1.277 | -1.253 | -1.246 |

| **M** | $b_1$ | | | | | | | | | | | | | | | |
|---|---|---|---|---|---|---|---|---|---|---|---|---|---|---|---|---|
| | 1.334 Hz | 1.778 Hz | 2.371 Hz | 3.162 Hz | 4.217 Hz | 5.623 Hz | 7.499 Hz | 10.000 Hz | 13.335 Hz | 17.783 Hz | 23.714 Hz | 31.623 Hz | 42.170 Hz | 56.234 Hz | 74.989 Hz | 100.000 Hz |
| 3.5 | -0.983 | -1.017 | -1.069 | -1.112 | -1.154 | -1.181 | -1.207 | -1.235 | -1.250 | -1.255 | -1.222 | -1.175 | -1.154 | -1.132 | -1.116 | -1.123 |
| 4 | -1.064 | -1.093 | -1.139 | -1.182 | -1.199 | -1.206 | -1.230 | -1.235 | -1.234 | -1.227 | -1.196 | -1.159 | -1.133 | -1.120 | -1.123 | -1.116 |
| 4.5 | -1.120 | -1.152 | -1.170 | -1.191 | -1.191 | -1.195 | -1.209 | -1.206 | -1.206 | -1.201 | -1.168 | -1.131 | -1.117 | -1.113 | -1.108 | -1.097 |
| 5 | -1.175 | -1.188 | -1.195 | -1.185 | -1.187 | -1.171 | -1.172 | -1.167 | -1.154 | -1.140 | -1.105 | -1.088 | -1.078 | -1.074 | -1.076 | -1.081 |
| 5.5 | -1.212 | -1.198 | -1.196 | -1.174 | -1.153 | -1.149 | -1.141 | -1.115 | -1.107 | -1.090 | -1.063 | -1.048 | -1.050 | -1.057 | -1.061 | -1.069 |
| 6 | -1.223 | -1.193 | -1.187 | -1.164 | -1.139 | -1.129 | -1.141 | -1.133 | -1.112 | -1.094 | -1.077 | -1.066 | -1.078 | -1.075 | -1.081 | -1.077 |
| 6.5 | -1.216 | -1.196 | -1.178 | -1.173 | -1.162 | -1.158 | -1.154 | -1.149 | -1.127 | -1.105 | -1.089 | -1.085 | -1.085 | -1.100 | -1.098 | -1.092 |
| 7 | -1.214 | -1.190 | -1.181 | -1.167 | -1.148 | -1.154 | -1.147 | -1.129 | -1.104 | -1.102 | -1.081 | -1.075 | -1.087 | -1.092 | -1.091 | -1.092 |
| 7.5 | -1.218 | -1.192 | -1.189 | -1.169 | -1.167 | -1.165 | -1.152 | -1.135 | -1.123 | -1.104 | -1.087 | -1.077 | -1.084 | -1.081 | -1.084 | -1.082 |
| 8 | -1.214 | -1.192 | -1.181 | -1.174 | -1.165 | -1.158 | -1.150 | -1.134 | -1.101 | -1.085 | -1.063 | -1.064 | -1.071 | -1.071 | -1.073 | -1.073 |

Table 3. Crustal-amplification factors (Boore and Thompson, 2015)

| CENA (used for Gulf coast region in this study) Table 4 of Thompson and Boore (2015) | | WNA Table 3 of Thompson and Boore (2015) | |
|---|---|---|---|
| *f* (Hz) | *A(f)* | *f* (Hz) | *A(f)* |
| 1.00E-03 | 1.000 | 1.00E-03 | 1.00 |
| 7.83E-03 | 1.003 | 9.00E-03 | 1.01 |
| 2.33E-02 | 1.010 | 2.50E-02 | 1.03 |
| 4.00E-02 | 1.017 | 4.90E-02 | 1.06 |
| 6.14E-02 | 1.026 | 8.10E-02 | 1.10 |
| 1.08E-01 | 1.047 | 1.50E-01 | 119 |
| 2.34E-01 | 1.069 | 3.70E-01 | 1.39 |
| 3.45E-01 | 1.084 | 6.80E-01 | 1.58 |
| 5.08E-01 | 1.101 | 1.11E+00 | 1.77 |
| 1.09E+00 | 1.135 | 2.36E+00 | 2.24 |
| 1.37E+00 | 1.143 | 5.25E+00 | 2.75 |
| 1.69E+00 | 1.148 | 6.03E+01 | 4.49 |
| 1.97E+00 | 1.150 | 1.00E+02 | 4.49 |

Note: Crustal-amplification factor do not include the effects of site attenuation.

Table 4. Coefficients and standard deviations of regression for the stochastic-scaling approach

| T(s) | **c1** | c2 | c3 | c4 | c5 | c6 | c7 | c8 | c9 | c10 | c11 | σReg |
|---|---|---|---|---|---|---|---|---|---|---|---|---|
| PGA | -1.2629503 | 0.4617977 | -0.0446316 | -4.0478962 | 0.4777507 | 0.8367772 | -0.1200742 | -0.2235040 | 0.0274395 | -0.0031319 | 3.4950815 | 0.1171473 |
| 1.00E-02 | -1.6653767 | 0.5944734 | -0.0542137 | -4.0485737 | 0.4846252 | 0.8239694 | -0.1187228 | -0.2194794 | 0.0272113 | -0.0031343 | 3.4347732 | 0.1087795 |
| 2.00E-02 | -2.1677451 | 0.7671877 | -0.0682192 | -4.0715809 | 0.4899226 | 0.8766151 | -0.1258817 | -0.2059501 | 0.0262428 | -0.0031847 | 3.3976406 | 0.0969845 |
| 3.00E-02 | -2.7953657 | 0.9750047 | -0.0845785 | -4.0158056 | 0.4855421 | 1.0247871 | -0.1449664 | -0.1581486 | 0.0225816 | -0.0032959 | 3.3283506 | 0.0858431 |
| 4.00E-02 | -2.8464568 | 1.0081002 | -0.0881682 | -3.9653988 | 0.4831417 | 1.1038879 | -0.1507431 | -0.0910483 | 0.0195180 | -0.0034530 | 3.2813584 | 0.0775443 |
| 5.00E-02 | -2.6853666 | 0.9827377 | -0.0879426 | -3.9470667 | 0.4837852 | 1.0565620 | -0.1374174 | -0.0078891 | 0.0159870 | -0.0036219 | 3.2634049 | 0.0733876 |
| 7.50E-02 | -2.2744368 | 0.9212777 | -0.0858807 | -3.8870199 | 0.4774107 | 0.7237267 | -0.0821028 | 0.2275315 | -0.0044707 | -0.0040944 | 3.2383728 | 0.0747710 |
| 1.00E-01 | -2.4001516 | 1.0153304 | -0.0949217 | -3.8265838 | 0.4662592 | 0.4352901 | -0.0433470 | 0.3274683 | -0.0207128 | -0.0043059 | 3.2163084 | 0.0843904 |
| 1.50E-01 | -2.8045756 | 1.1682462 | -0.1056039 | -3.7203204 | 0.4445391 | 0.1895793 | -0.0212540 | 0.1658353 | -0.0144212 | -0.0041061 | 3.1526837 | 0.1085784 |
| 2.00E-01 | -3.2454183 | 1.3019814 | -0.1154654 | -3.6690351 | 0.4335515 | 0.1543138 | -0.0271627 | -0.1235750 | 0.0128548 | -0.0035628 | 3.1668459 | 0.1268362 |
| 2.50E-01 | -3.5180537 | 1.3541275 | -0.1182048 | -3.6130223 | 0.4229366 | 0.1784055 | -0.0388452 | -0.3777475 | 0.0391632 | -0.0029471 | 3.1730250 | 0.1363620 |
| 3.00E-01 | -3.5125403 | 1.3033903 | -0.1122576 | -3.5424387 | 0.4115696 | 0.2056076 | -0.0487656 | -0.5739290 | 0.0600759 | -0.0024576 | 3.1653083 | 0.1300102 |
| 4.00E-01 | -3.8417319 | 1.3239390 | -0.1105367 | -3.4722998 | 0.4000348 | 0.2542473 | -0.0634595 | -0.8319918 | 0.0878387 | -0.0014996 | 3.1418072 | 0.1230800 |
| 5.00E-01 | -3.9577764 | 1.2866198 | -0.1043854 | -3.4166350 | 0.3910215 | 0.2785803 | -0.0714092 | -0.9820135 | 0.1039002 | -0.0010161 | 3.1183660 | 0.1171632 |
| 7.50E-01 | -4.5160690 | 1.3141845 | -0.1000153 | -3.3477564 | 0.3813472 | 0.2933157 | -0.0792270 | -1.1621982 | 0.1226756 | -0.0007447 | 3.0662005 | 0.0957211 |
| 1.00E+00 | -4.8432629 | 1.3242465 | -0.0973946 | -3.2787097 | 0.3715118 | 0.2878724 | -0.0811981 | -1.2457085 | 0.1308101 | -0.0007823 | 3.0584551 | 0.0905270 |
| 1.50E+00 | -5.0254440 | 1.2615612 | -0.0889666 | -3.2322430 | 0.3642532 | 0.2913337 | -0.0844144 | -1.3289086 | 0.1375912 | -0.0007062 | 3.1173369 | 0.0915098 |
| 2.00E+00 | -5.1913711 | 1.2303899 | -0.0844070 | -3.2231738 | 0.3615307 | 0.3076508 | -0.0881380 | -1.3757692 | 0.1403730 | -0.0006085 | 3.2168228 | 0.0908361 |
| 3.00E+00 | -5.2432312 | 1.1068165 | -0.0702874 | -3.2834862 | 0.3664648 | 0.3314988 | -0.0960349 | -1.4487584 | 0.1420152 | -0.0004698 | 3.3940312 | 0.0926133 |
| 4.00E+00 | -5.3271547 | 1.0438491 | -0.0626062 | -3.3941089 | 0.3771293 | 0.3605776 | -0.1052715 | -1.5052923 | 0.1415896 | -0.0002702 | 3.5111602 | 0.0942376 |
| 5.00E+00 | -5.6675338 | 1.0675728 | -0.0617984 | -3.4636561 | 0.3872566 | 0.4196719 | -0.1139869 | -1.5173139 | 0.1402061 | -0.0002809 | 3.5573198 | 0.0936410 |
| 7.50E+00 | -6.3183320 | 1.0778146 | -0.0571083 | -3.3803692 | 0.3889195 | 0.6569113 | -0.1347036 | -1.4282726 | 0.1351004 | -0.0003010 | 3.5309571 | 0.0999430 |
| 1.00E+01 | -6.9758145 | 1.1328486 | -0.0573196 | -3.3336355 | 0.3926830 | 0.9574895 | -0.1637387 | -1.2808301 | 0.1244957 | -0.0003263 | 3.4685770 | 0.1106370 |

Table 5. Coefficients of the τ variability model in natural log units

| T (sec) | C12 | C13 | C14 | C15 | C16 | C17 | C18 |
|---|---|---|---|---|---|---|---|
| PGA | 4.191074E-01 | 7.699011E-01 | -7.797671E-02 | 5.517730E-01 | -3.435110E-02 | 3.596377E-01 | -4.791813E-03 |
| 0.010 | 4.188574E-01 | 7.505261E-01 | -7.372671E-02 | 5.598980E-01 | -3.560110E-02 | 3.596377E-01 | -4.791813E-03 |
| 0.020 | 4.245110E-01 | 8.034037E-01 | -8.422056E-02 | 5.569298E-01 | -3.492580E-02 | 3.610473E-01 | -4.790018E-03 |
| 0.030 | 4.416215E-01 | 8.783665E-01 | -9.708683E-02 | 5.700579E-01 | -3.542510E-02 | 3.715501E-01 | -4.885450E-03 |
| 0.040 | 4.572109E-01 | 9.425545E-01 | -1.079171E-01 | 5.735656E-01 | -3.411934E-02 | 3.853471E-01 | -5.162642E-03 |
| 0.050 | 4.727015E-01 | 1.006637E+00 | -1.187477E-01 | 5.771759E-01 | -3.285558E-02 | 3.990010E-01 | -5.444060E-03 |
| 0.075 | 4.655489E-01 | 7.718243E-01 | -6.819065E-02 | 5.842607E-01 | -3.067792E-02 | 4.218630E-01 | -5.693666E-03 |
| 0.100 | 4.371127E-01 | 4.594151E-01 | -5.077560E-03 | 5.919743E-01 | -3.158939E-02 | 4.230738E-01 | -5.604700E-03 |
| 0.150 | 4.080820E-01 | 3.550683E-01 | 1.173359E-02 | 5.801798E-01 | -3.328870E-02 | 3.962444E-01 | -4.990958E-03 |
| 0.200 | 3.959781E-01 | 4.397503E-01 | -9.743777E-03 | 5.796868E-01 | -3.773109E-02 | 3.650475E-01 | -4.709655E-03 |
| 0.250 | 3.984569E-01 | 5.748189E-01 | -3.920435E-02 | 5.772845E-01 | -3.969747E-02 | 3.497345E-01 | -4.689783E-03 |
| 0.300 | 4.022762E-01 | 6.887418E-01 | -6.366886E-02 | 5.822120E-01 | -4.236289E-02 | 3.372350E-01 | -4.674133E-03 |
| 0.400 | 4.116224E-01 | 9.149968E-01 | -1.118671E-01 | 5.601217E-01 | -4.089205E-02 | 3.245592E-01 | -4.651665E-03 |
| 0.500 | 4.252078E-01 | 1.026316E+00 | -1.335837E-01 | 5.581676E-01 | -3.995393E-02 | 3.286064E-01 | -4.636830E-03 |
| 0.750 | 4.507188E-01 | 1.016755E+00 | -1.257874E-01 | 5.932706E-01 | -4.109052E-02 | 3.561638E-01 | -4.612542E-03 |
| 1.000 | 4.715970E-01 | 1.091562E+00 | -1.377708E-01 | 6.055414E-01 | -4.056668E-02 | 3.717735E-01 | -4.602390E-03 |
| 1.500 | 4.858731E-01 | 1.052939E+00 | -1.260151E-01 | 6.366955E-01 | -4.276645E-02 | 3.886223E-01 | -4.601346E-03 |
| 2.000 | 4.885966E-01 | 1.051221E+00 | -1.250285E-01 | 6.359337E-01 | -4.197110E-02 | 3.931833E-01 | -4.624890E-03 |
| 3.000 | 4.906976E-01 | 9.880408E-01 | -1.105213E-01 | 6.468676E-01 | -4.228672E-02 | 4.020789E-01 | -4.626913E-03 |
| 4.000 | 5.033497E-01 | 1.227861E+00 | -1.610025E-01 | 6.062061E-01 | -3.667159E-02 | 3.976729E-01 | -4.589560E-03 |
| 5.000 | 4.986000E-01 | 1.101600E+00 | -1.340000E-01 | 6.311000E-01 | -3.990000E-02 | 4.015417E-01 | -4.583333E-03 |
| 7.500 | 4.910250E-01 | 1.049025E+00 | -1.240000E-01 | 6.579417E-01 | -4.578333E-02 | 3.901417E-01 | -4.583333E-03 |
| 10.000 | 4.710500E-01 | 8.445500E-01 | -8.300000E-02 | 6.848000E-01 | -5.105000E-02 | 3.827667E-01 | -4.583333E-03 |

Table 6. Coefficients of the $\phi$ variability model in natural log units

| T (sec) | C19 | C20 | C21 | C22 | C23 | C24 | C25 |
|---|---|---|---|---|---|---|---|
| 0.000 | 7.7158E-01 | -1.4751E-02 | 1.8796E+00 | -2.6098E-01 | 7.8483E-01 | -4.2026E-02 | 5.1159E-01 |
| 0.010 | 7.7191E-01 | -1.4751E-02 | 1.8788E+00 | -2.6073E-01 | 7.8487E-01 | -4.1942E-02 | 5.1217E-01 |
| 0.020 | 7.7603E-01 | -1.5122E-02 | 1.8858E+00 | -2.6174E-01 | 7.8887E-01 | -4.2351E-02 | 5.1351E-01 |
| 0.030 | 7.9486E-01 | -1.6494E-02 | 1.9255E+00 | -2.6774E-01 | 8.0967E-01 | -4.4579E-02 | 5.1980E-01 |
| 0.040 | 8.1036E-01 | -1.7316E-02 | 1.9741E+00 | -2.7593E-01 | 8.2244E-01 | -4.5593E-02 | 5.2588E-01 |
| 0.050 | 8.2542E-01 | -1.8163E-02 | 2.0223E+00 | -2.8413E-01 | 8.3462E-01 | -4.6601E-02 | 5.3142E-01 |
| 0.075 | 8.2645E-01 | -1.7821E-02 | 1.9672E+00 | -2.7132E-01 | 8.3628E-01 | -4.5138E-02 | 5.4248E-01 |
| 0.100 | 8.2100E-01 | -1.7142E-02 | 1.8703E+00 | -2.5031E-01 | 8.4160E-01 | -4.4577E-02 | 5.5145E-01 |
| 0.150 | 8.1653E-01 | -1.5352E-02 | 1.8545E+00 | -2.4602E-01 | 8.3445E-01 | -4.2004E-02 | 5.6126E-01 |
| 0.200 | 8.0776E-01 | -1.4127E-02 | 1.7701E+00 | -2.2797E-01 | 8.3132E-01 | -4.0224E-02 | 5.6980E-01 |
| 0.250 | 7.9127E-01 | -1.2596E-02 | 1.6894E+00 | -2.1219E-01 | 8.1265E-01 | -3.6831E-02 | 5.7320E-01 |
| 0.300 | 7.6503E-01 | -1.0073E-02 | 1.4753E+00 | -1.6790E-01 | 8.0211E-01 | -3.3274E-02 | 5.8579E-01 |
| 0.400 | 7.2553E-01 | -6.8569E-03 | 1.1547E+00 | -1.0223E-01 | 7.8939E-01 | -2.9166E-02 | 5.9978E-01 |
| 0.500 | 6.9780E-01 | -4.7789E-03 | 9.1289E-01 | -5.2576E-02 | 7.7712E-01 | -2.5424E-02 | 6.1185E-01 |
| 0.750 | 6.4414E-01 | -1.0108E-03 | 5.1149E-01 | 2.8467E-02 | 7.3937E-01 | -1.7109E-02 | 6.2815E-01 |
| 1.000 | 6.0866E-01 | 1.3073E-03 | 3.5643E-01 | 5.7358E-02 | 6.8131E-01 | -7.6173E-03 | 6.3179E-01 |
| 1.500 | 5.6530E-01 | 3.8718E-03 | 2.4077E-01 | 7.5988E-02 | 5.9578E-01 | 4.9859E-03 | 6.2818E-01 |
| 2.000 | 5.4428E-01 | 5.9319E-03 | 2.1502E-01 | 7.9103E-02 | 5.5740E-01 | 1.0625E-02 | 6.2645E-01 |
| 3.000 | 5.4144E-01 | 5.7462E-03 | 2.4787E-01 | 7.0984E-02 | 5.5048E-01 | 1.0462E-02 | 6.1846E-01 |
| 4.000 | 5.2943E-01 | 6.4371E-03 | 2.8221E-01 | 6.1373E-02 | 5.2868E-01 | 1.2080E-02 | 6.0720E-01 |
| 5.000 | 5.0999E-01 | 7.8125E-03 | 2.0371E-01 | 7.5875E-02 | 5.1224E-01 | 1.4168E-02 | 6.0434E-01 |
| 7.500 | 4.6975E-01 | 1.0813E-02 | -1.6528E-02 | 1.1888E-01 | 4.9201E-01 | 1.7168E-02 | 6.0360E-01 |
| 10.000 | 4.5114E-01 | 1.2562E-02 | -5.5396E-02 | 1.2513E-01 | 4.8980E-01 | 1.6085E-02 | 5.9436E-01 |

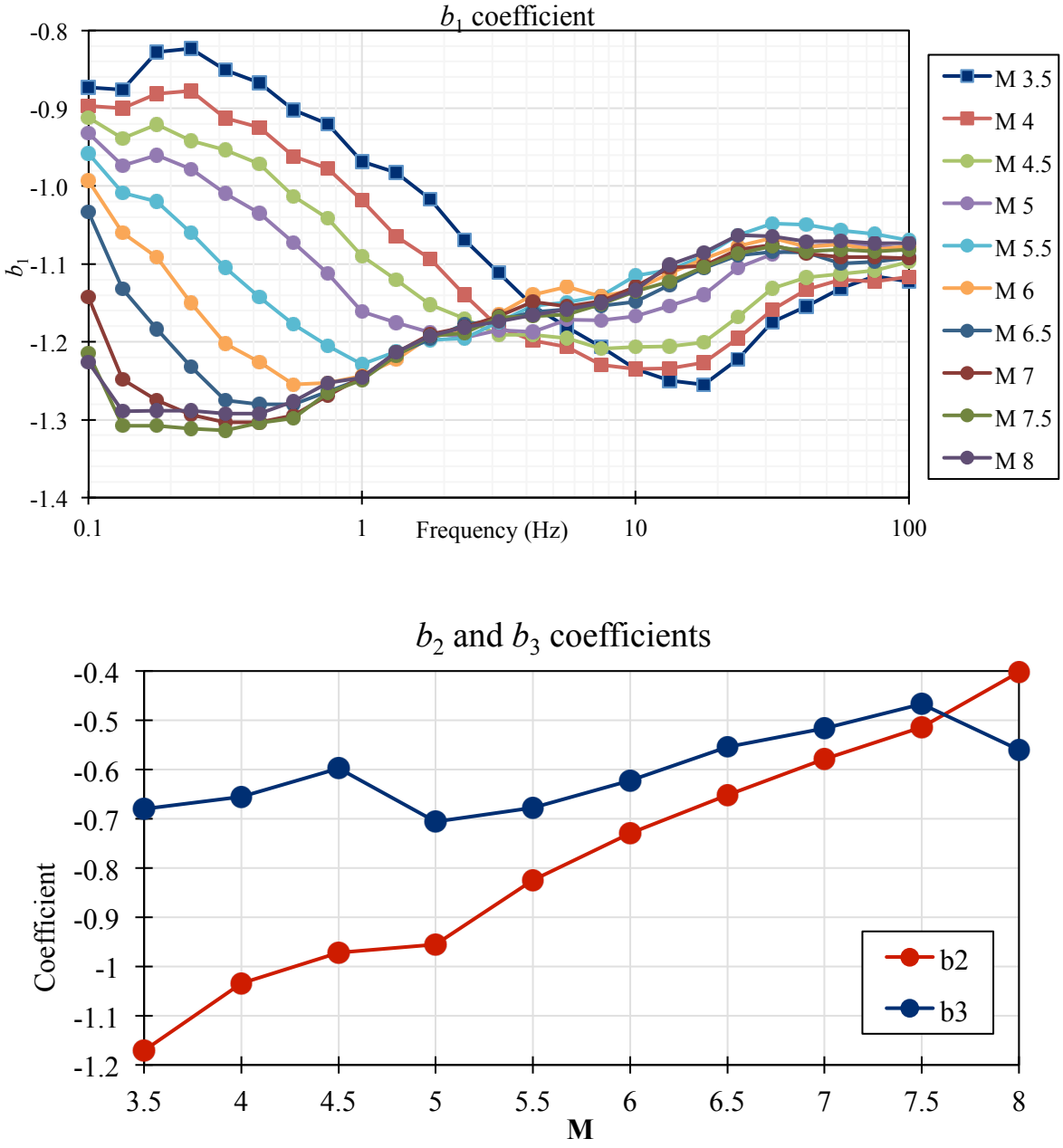


*Figure 1. Geometrical spreading coefficients obtained from the GA inversion of the NGA-West2 GMPEs: (a) coefficient $b_1$ as a function of magnitude and frequency; (b) coefficients $b_2$ and $b_3$ as a function of magnitude (Source: Zandieh et al. (2017)).*

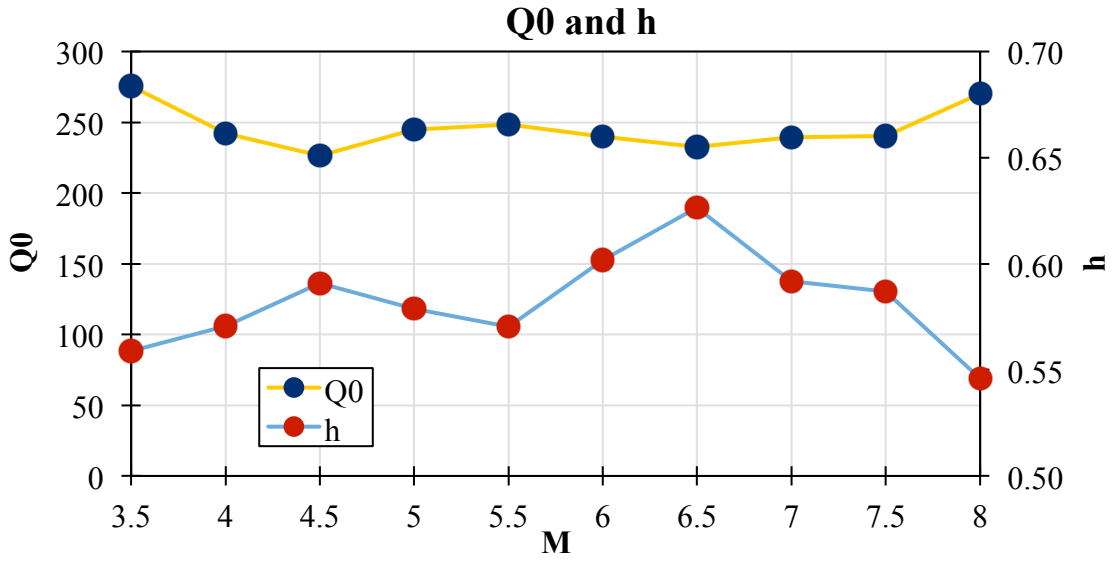


*Figure 2. Anelastic attenuation parameters and model obtained from the GA inversion of the NGA-West2 GMPEs: (a) parameters $Q_0$ and $\eta$ as a function of magnitude; (b) the quality factor function $Q(f) = Q_0 f^{\eta}$ for different magnitudes as a function of frequency (Source: Zandieh et al. (2017)).*

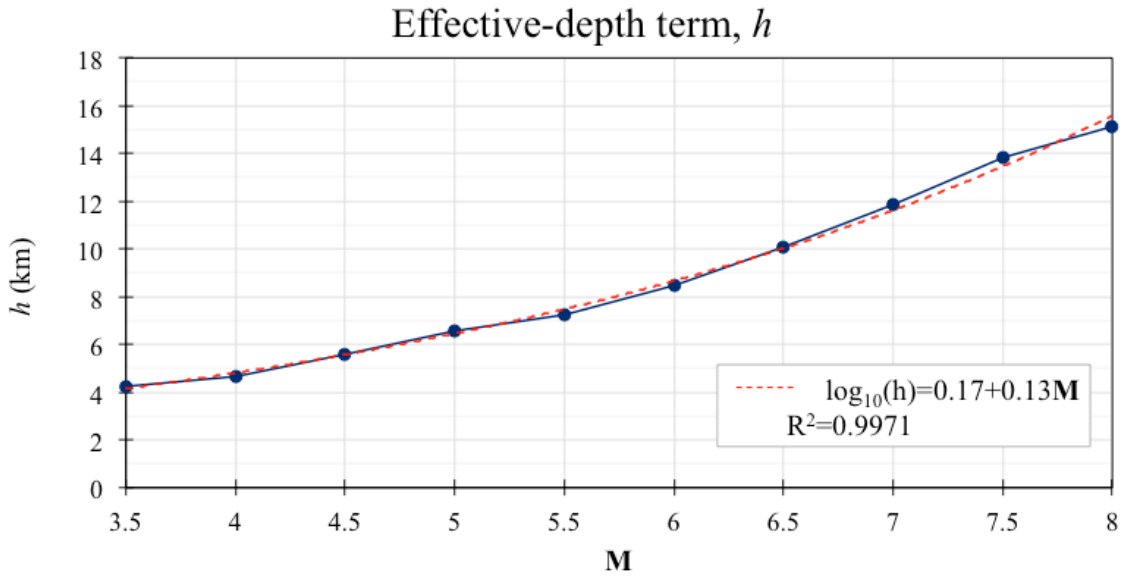


*Figure 3. Effective-depth term, h(**M**) obtained from the GA inversion of the NGA-West2 GMPEs along with a fitted functional form given by the equation log(h(**M**)) = a+b**M** (Source: Zandieh et al. (2017)).*

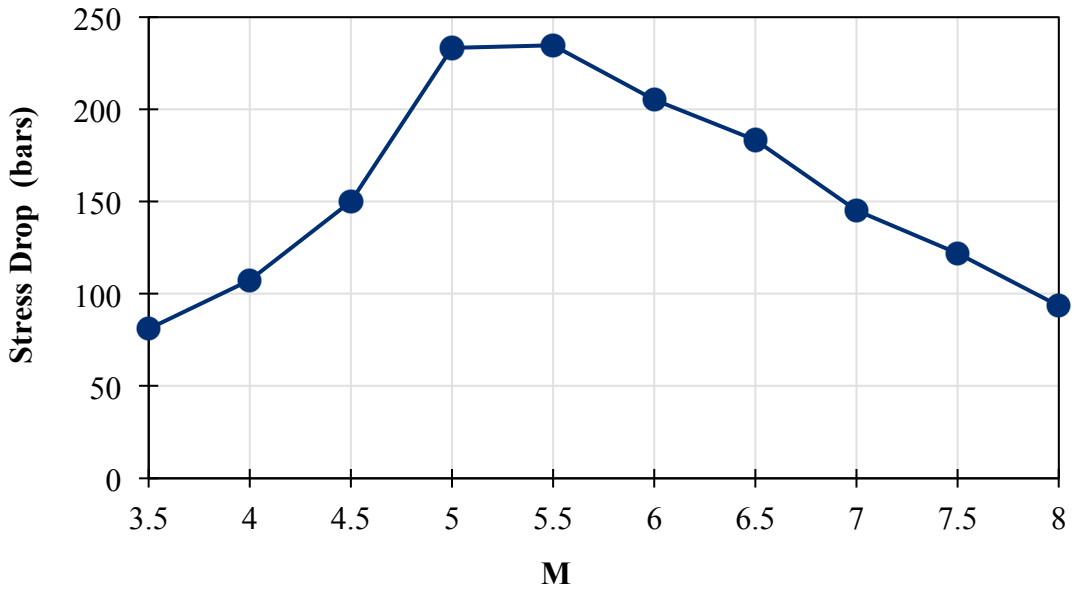


*Figure 4. Stress parameter $\Delta\sigma$ values obtained from GA inversion of the NGA-West2 GMPEs as a function of magnitude.*

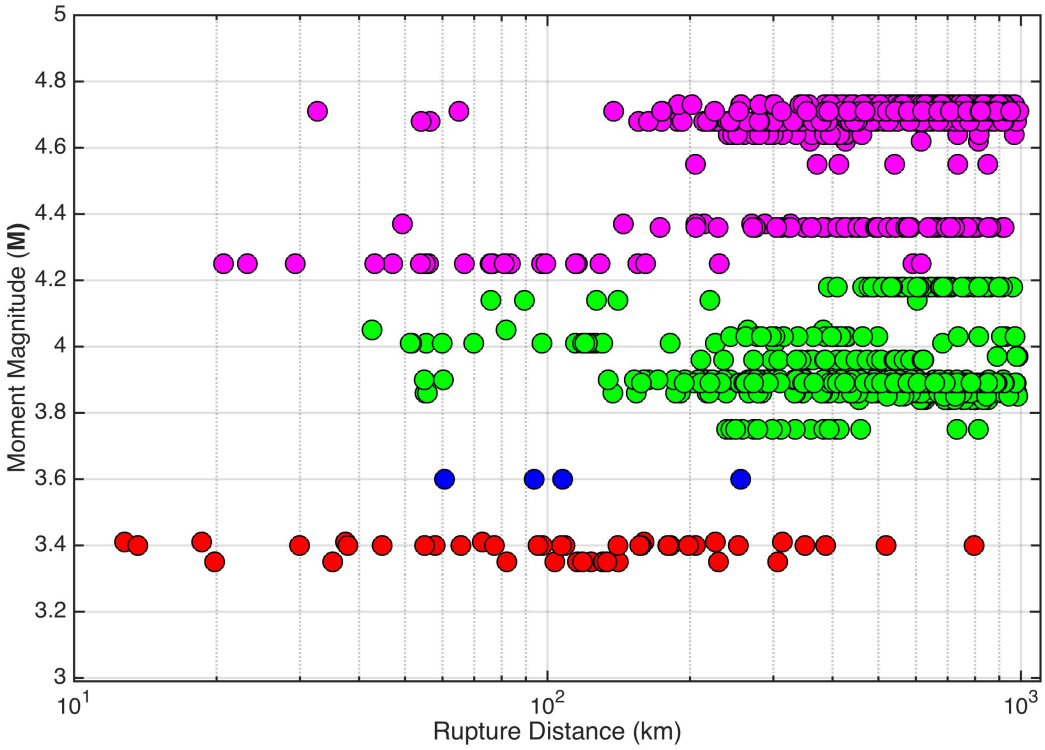


Figure 5. *The magnitude–distance distribution of the selected ground-motion recordings within the Gulf Coast region.*

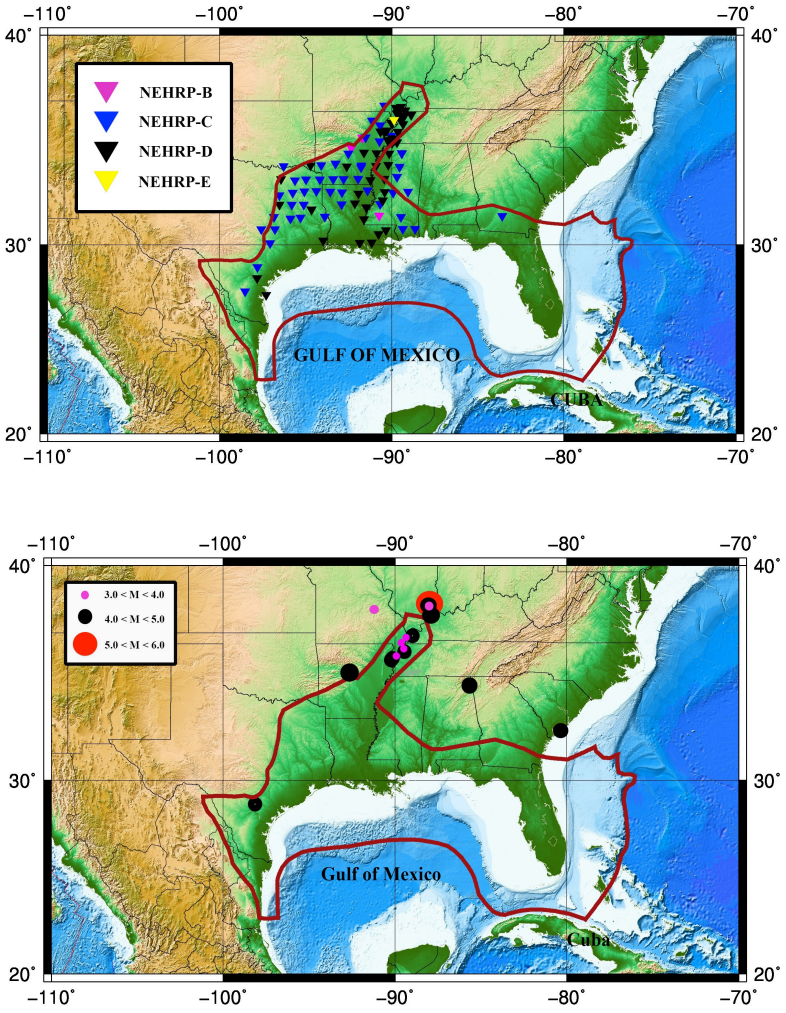


*Figure 6. (Left): Recording stations within the Gulf Coast region. The colors of the symbols represent the NEHRP site class of the station; (Right): The Gulf Coast region earthquakes considered in this study.*

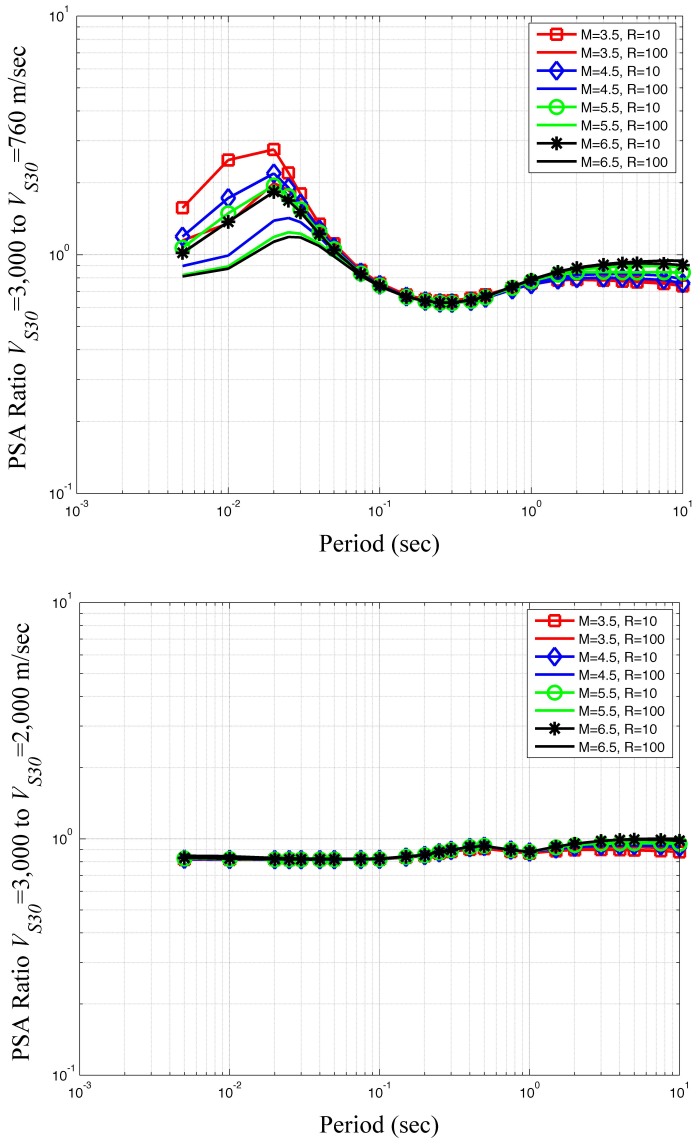


*Figure 7. Comparisons of the $V_{S30}$=3000 m/sec to NEHRP B/C ($V_{S30}$ = 760 m/sec) PSA spectral ratios (top) and the $V_{S30}$ = 3000 to $V_{S30}$ = 2000 m/sec PSA spectral ratios (bottom) used to adjust the empirical observations to the CENA reference hard-rock site condition recommended by Hashash et al. (2014a).*

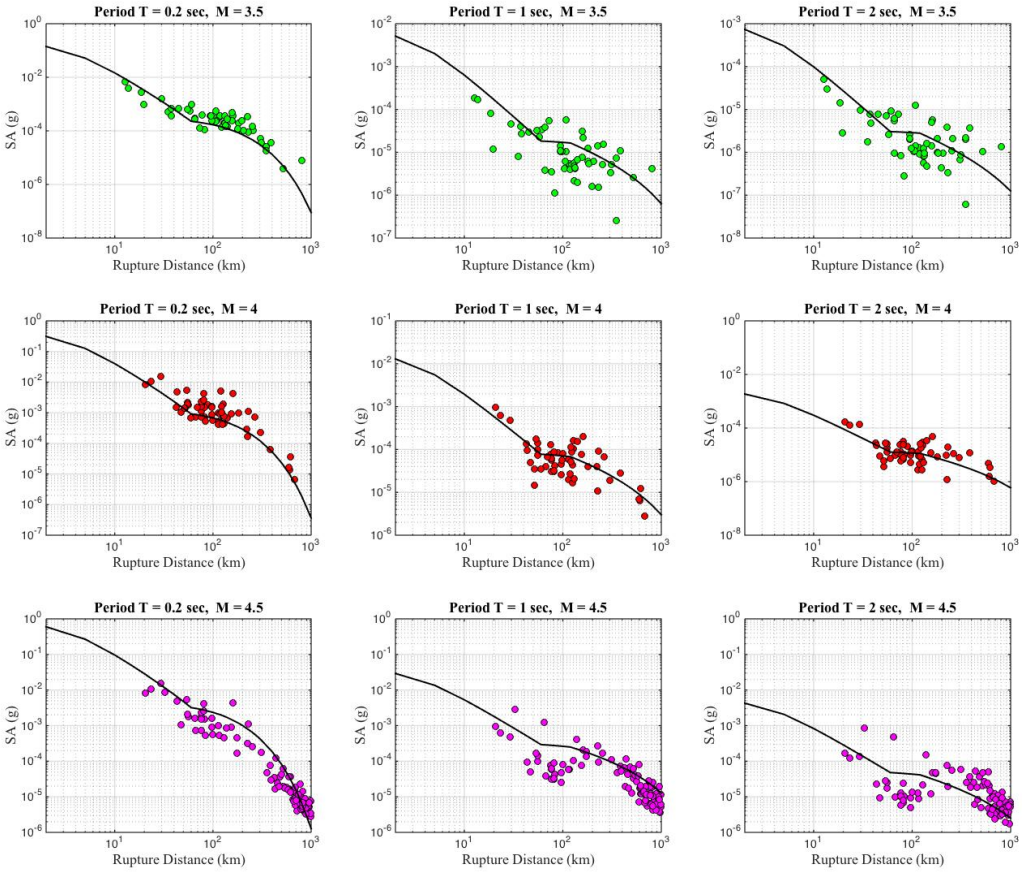


*Figure 8. Comparisons of the GMIM predictions from the hybrid empirical ground motion prediction equation developed in this study with the site-adjusted GMIM observations for spectral periods of 0.2, 1.0, and 2.0 sec and three magnitude bins:* ***M*** *= 3.5 (3.25–3.75),* ***M*** *= 4.0 (3.75–4.25), and* ***M*** *= 4.5 (4.25–4.75).*

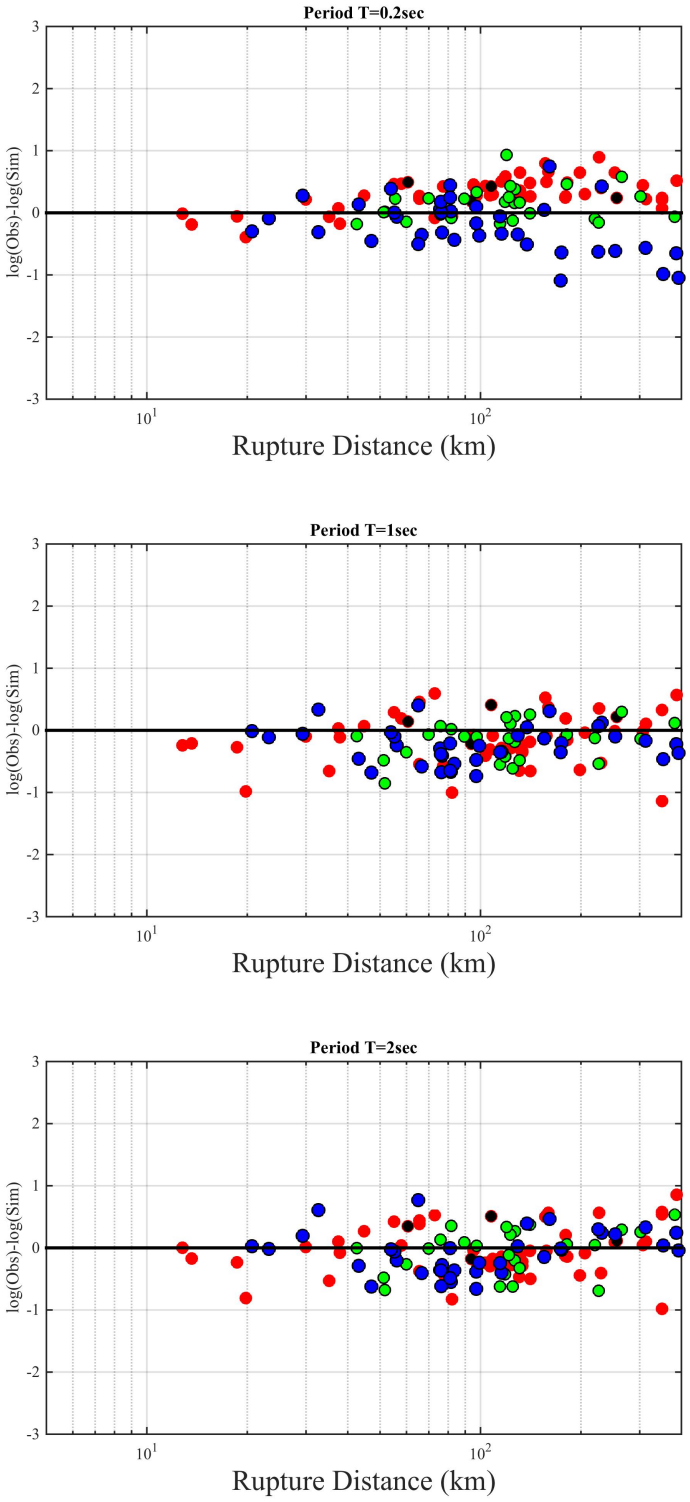


*Figure 9. Plots showing the distribution of the site-adjusted residuals as a function of rupture distance ($R_{RUP}$). The size of each circle and its shades represent the magnitude of the event. The squares represent the mean binned the binned residuals.*

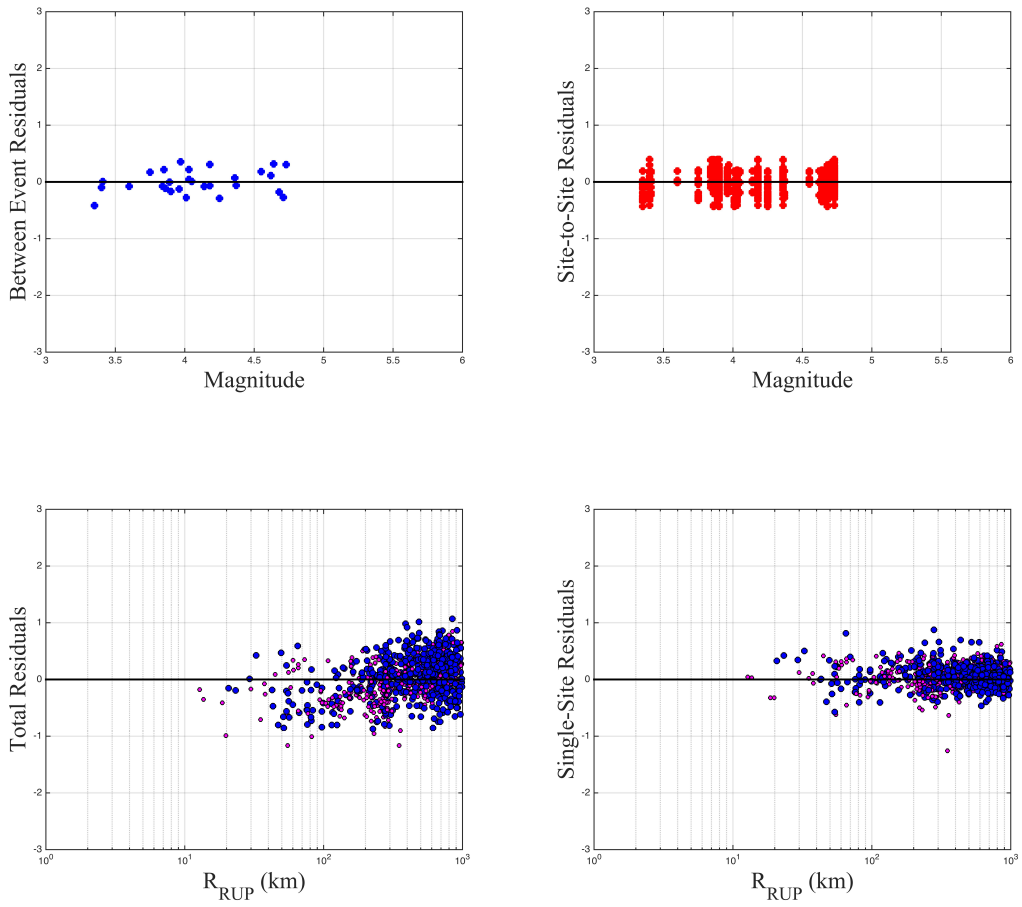


*Figure 10. Plots showing the between-event residuals versus magnitude (upper left), the within-event residuals versus magnitude (upper right), the total residuals versus rupture distance (lower left), and the within-event single-site residuals versus rupture distance (lower right) for a spectral period of 1.0 sec. The size of each circle and its shades represent the magnitude of the event.*

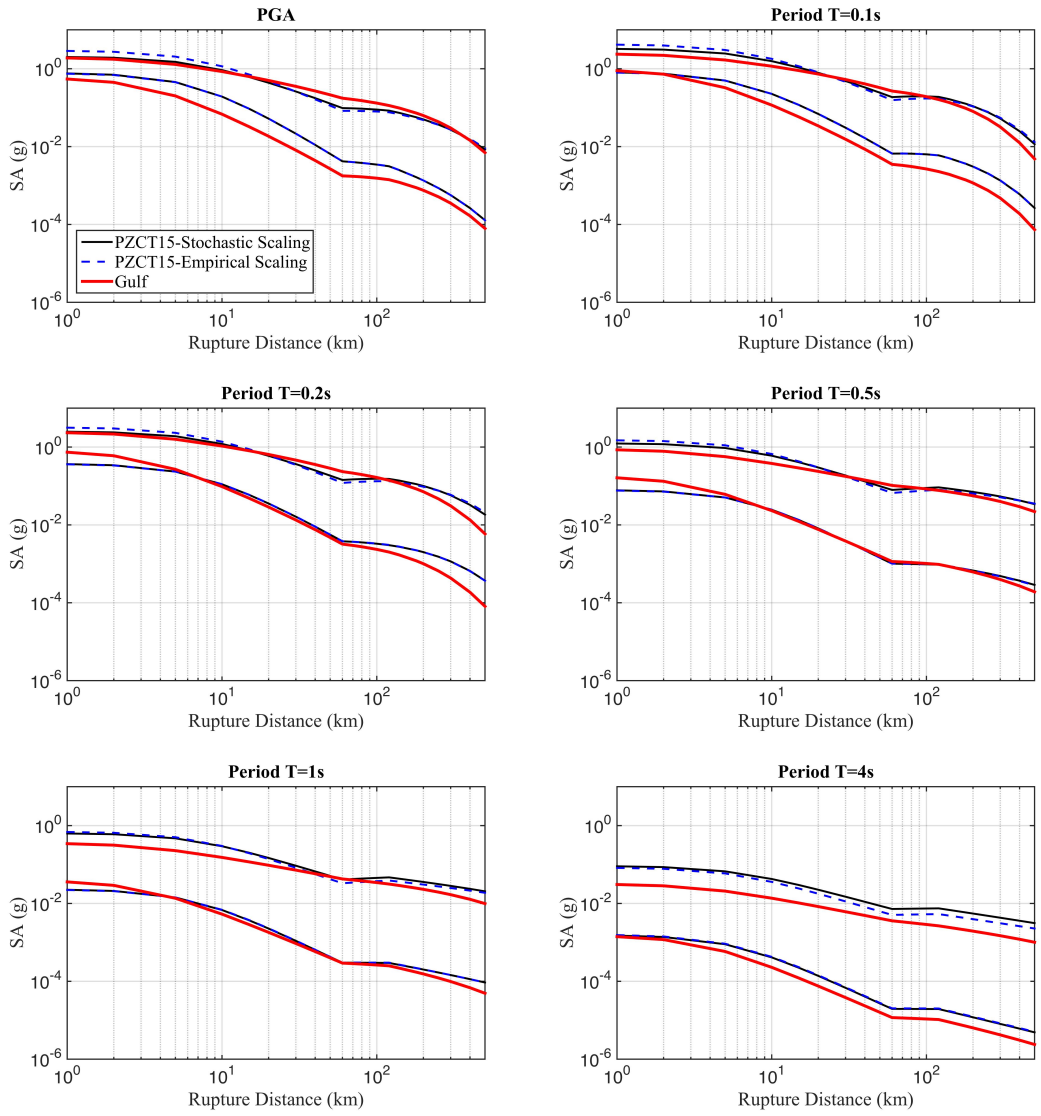


*Figure 5. Comparison of PGA and PSA predicted by the CENA ground motion prediction equations developed in this study with the predictions of two hybrid empirical models by Pezeshk et al. (2015): (lower curve)* ***M*** *= 4.5; (upper curve)* ***M*** *= 7.*

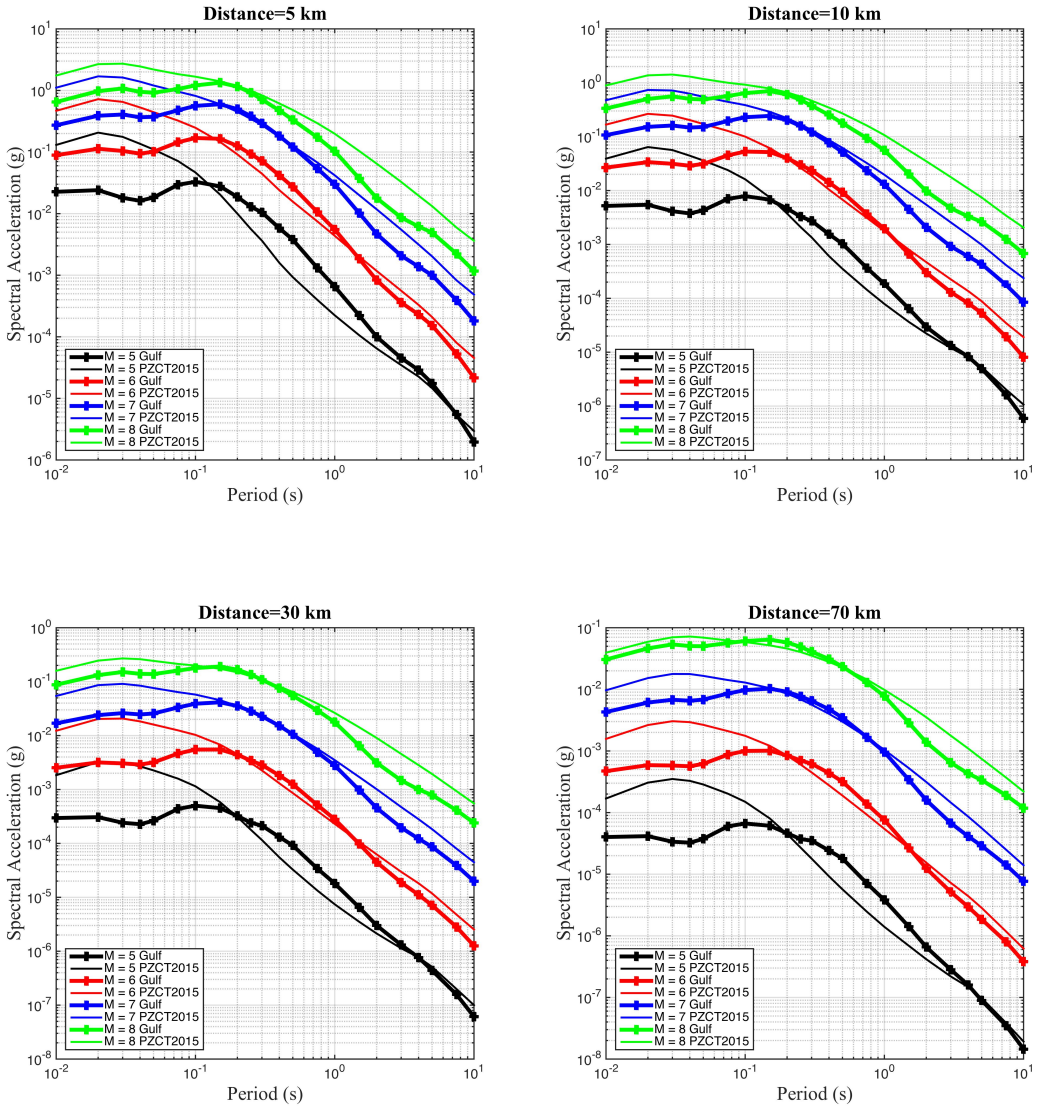


Figure 11. Response spectra predicted by the CENA hybrid empirical ground motion prediction equation developed in this study based on the stochastic-scaling approach to large-magnitude scaling showing its dependence on magnitude at rupture distances ($R_{RUP}$) of 5, 10, 30, and 70 km.